Assessment of Remote Sensing Technologies for Location of Hydrogen and Helium Leaks

NAG10-0290

Phase 2 Final Report

31 October 2001

R. Glenn Sellar
Yongho Sohn
Varun Mathur
Peter Reardon

This research was supported by the NASA Kennedy Space Center
under grant # NAG10-0290

Florida Space Institute

TABLE OF CONTENTS

1 EXECUTIVE SUMMARY

In Phase 1 of this project, a hierarchy of techniques for H_2 and He leak location was developed (see Figure 1). A total of twelve specific remote sensing techniques were evaluated; the results are summarized in Table 1. A basic diffusion model was also developed to predict the concentration and distribution of H_2 or He resulting from a leak.

1.1 Phase 2 Objectives

The objectives of Phase 2 of the project consisted of the following four tasks:

1.1.1 Advance Rayleigh Doppler technique from TRL 1 to TRL 2

The first task was to advance the Rayleigh Doppler technique from Technology Readiness Level (TRL) 2 to TRL 3 by developing a theoretical model. The result of this task is an interactive model that provides expected signal-to-noise ratio as a function of key design parameters.

1.1.2 Plan to advance Rayleigh Doppler technique from TRL 2 to TRL 3

The second task was to design and estimate the cost for an experiment intended to advance the Rayleigh Doppler technique from TRL 2 to TRL 3. The result of this task is a design for the experimental apparatus, and a parts list including costs.

1.1.3 Identify researchers and resources for further advancement

The third task was to identify researchers, facilities and other resources that could contribute to the further advancement of this research.

1.1.4 Extend diffusion model

The fourth task was to extend the diffusion model developed in Phase 1 to apply to the following:

1) The case for diffusion into an enclosed volume;
2) Inclusion of the effect of forced convection; and
3) Inclusion of the effect of gravitational convection.

The result of this task is an interactive model of concentration as a function of position, for various leak parameters and environmental conditions.

1.2 Phase 2 Results

A theoretical model has been developed that predicts the signal-to-noise ratio as a function of the key design parameters. This model includes both direct detection and heterodyne detection.

Five approaches to the Rayleigh Doppler have been considered singly and in combination as candidates for a proof-of-principle experiment.

1) Heterodyne
   a) Homodyne
   b) Offset Homodyne
   c) Heterodyne
2) Vapor Absorption Filter
3) Fabry Perot

A survey of the key technologies for the laser, detector, modulator, filter, and frequency discriminator has indicated that two approaches may be currently feasible within the expected budget constraints for Phase 3: homodyne, and a combination of vapor absorption filter and Fabry-Perot. Analyses using the model developed in this phase indicate that *both* of these techniques are expected to provide signal-to-noise ratios suitable for proof-of-principle experiments.

Designs for these two experiments have been outlined, and the required parts have been listed. Several experts have been identified who may be helpful in pursuing further research, and their *curricula vita* are included in the report.

The concentration model developed in Phase 1 has been successfully extended to include the effects of gravitational convection and forced convection. This model is an essential tool for relating concentrations to leak rates.

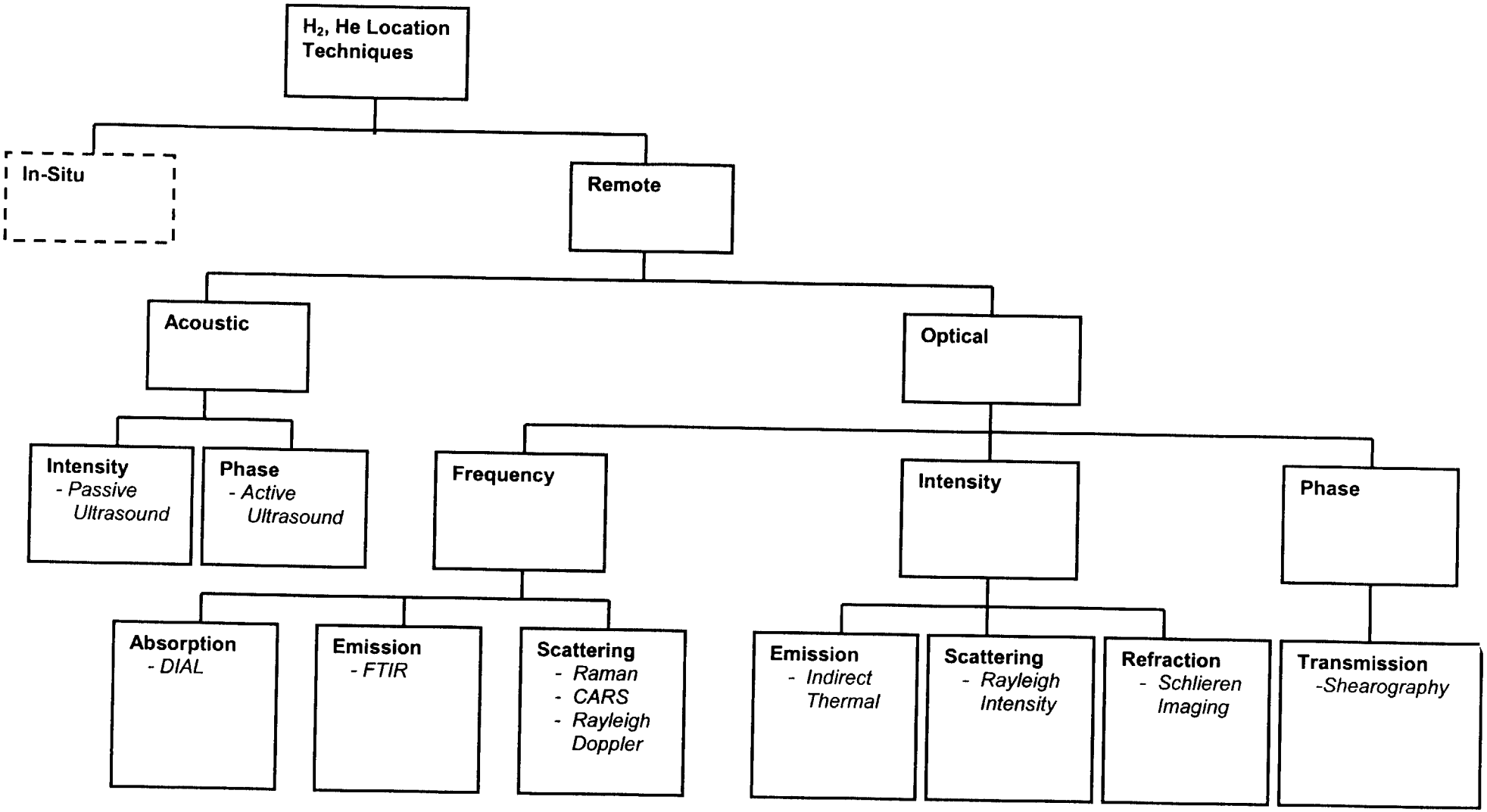

Figure 1: Hierarchy of H_2 & He Location Techniques

Table 1: Technology Evaluation Summary

Technique	**Distinguishing Characteristic**	**Measurement**	**Applicability**	**TRL**
Passive Sonar	Turbulent airflow (ultrasound)	Acoustic intensity (passive)	Demonstrated Low spatial resolution Sensitivity depends on pressure and aperture	4
Active Sonar	Speed of sound	Phase of acoustic waves (active)	Low spatial resolution Sensitivity limited by clutter	3
DIAL	Allowable energy levels	Absorption of radiation at characteristic wavelengths (active)	None – absorption lines only in vacuum UV	-
FTIR	Allowable energy levels	Emission of radiation at characteristic wavelengths (passive)	None – absorption lines only in vacuum UV	-
Raman - spontaneous	Allowable energy levels	Shift in wavelength of inelastically scattered radiation (active)	H_2: Sensitivity of 2% demonstrated *He*: None – monatomic therefore no vibration	6
Raman – CARS	Allowable energy levels	Shift in wavelength of inelastically scattered radiation (active)	H_2: Sensitivity of 10 ppm demonstrated *He*: None – monatomic therefore no vibration	3
Rayleigh Doppler	Molecular/atomic velocities	Shift in wavelength of elastically scattered radiation (active)	Theoretically applicable for both H_2 and He	1
Indirect Thermal	Temperature	Variation in temperature of solids caused by nearby cryogenic gas or expanding gas (passive)	Clutter limited?	3
Rayleigh Intensity	Molecular/atomic cross-section	Intensity of elastically scattered radiation (active)	Limited by Mie scattering (particulates) Clutter limited?	3
Schlieren	Index of refraction	Refraction of radiation caused by spatial variations in index of refraction (active)	Sensitivity limited by clutter: 1° ~ 346 ppm H_2 1° ~ 461 ppm He	4
Shearography	Index of refraction	Phase (path length) of transmitted radiation (active)	Sensitivity limited by clutter: 1° ~ 346 ppm H_2 1° ~ 461 ppm He	5

2 ADVANCE RAYLEIGH DOPPLER TECHNIQUE FROM TRL 1 TO TRL 2

2.1 Introduction

When electromagnetic radiation is emitted, scattered, or reflected from an object moving toward or away from an observer, the observed wavelength is shifted in what is known as the *Doppler effect*. The molecules of a gas will scatter electromagnetic radiation in what is known as *Rayleigh scattering*. Thus radiation that is Rayleigh scattered from a gas may be shifted in wavelength due to the velocity of the scattering molecules.

Mass m, speed v, and kinetic energy E_k, are related according to the following equation:

$$E_k = \frac{1}{2}mv^2$$

The distribution of kinetic energies of the molecules in a gas is independent of the *composition* of the gas, and depends only (to first order) on the *temperature* of the gas. But since different gases have different molecular masses, the distribution of *speeds* will vary with the composition of the gas.

Since the molecules in a gas move in a random distribution of velocities, when light of a single frequency is scattered from a gas the frequency spectrum of the scattered light is *broadened* in an effect known as *Doppler broadening*. The degree of broadening will be dependent on the velocities of the molecules, which in turn depends upon the composition of the gas. Thus it is possible to determine the composition of a gas by measuring the Doppler broadening of Rayleigh scattered light[1].

2.2 Theoretical model

The distribution of speeds is given by the Maxwell-Boltzmann distribution:

$$f(v) = 4\pi\left(\frac{m}{2\pi kT}\right)^{\frac{3}{2}} v^2 e^{\frac{-mv^2}{2kT}}$$

where $f(v)$ is the probability density (i.e. $f(v)\,\delta v$ is the fraction of molecules with velocity between v and $v+\delta v$), m is the mass of the molecule, k is the Stephan-Boltzmann constant, and T is the absolute temperature. The speed distributions for H_2, He, N_2 and O_2 at 293 K (room temperature) are shown in Figure 2.

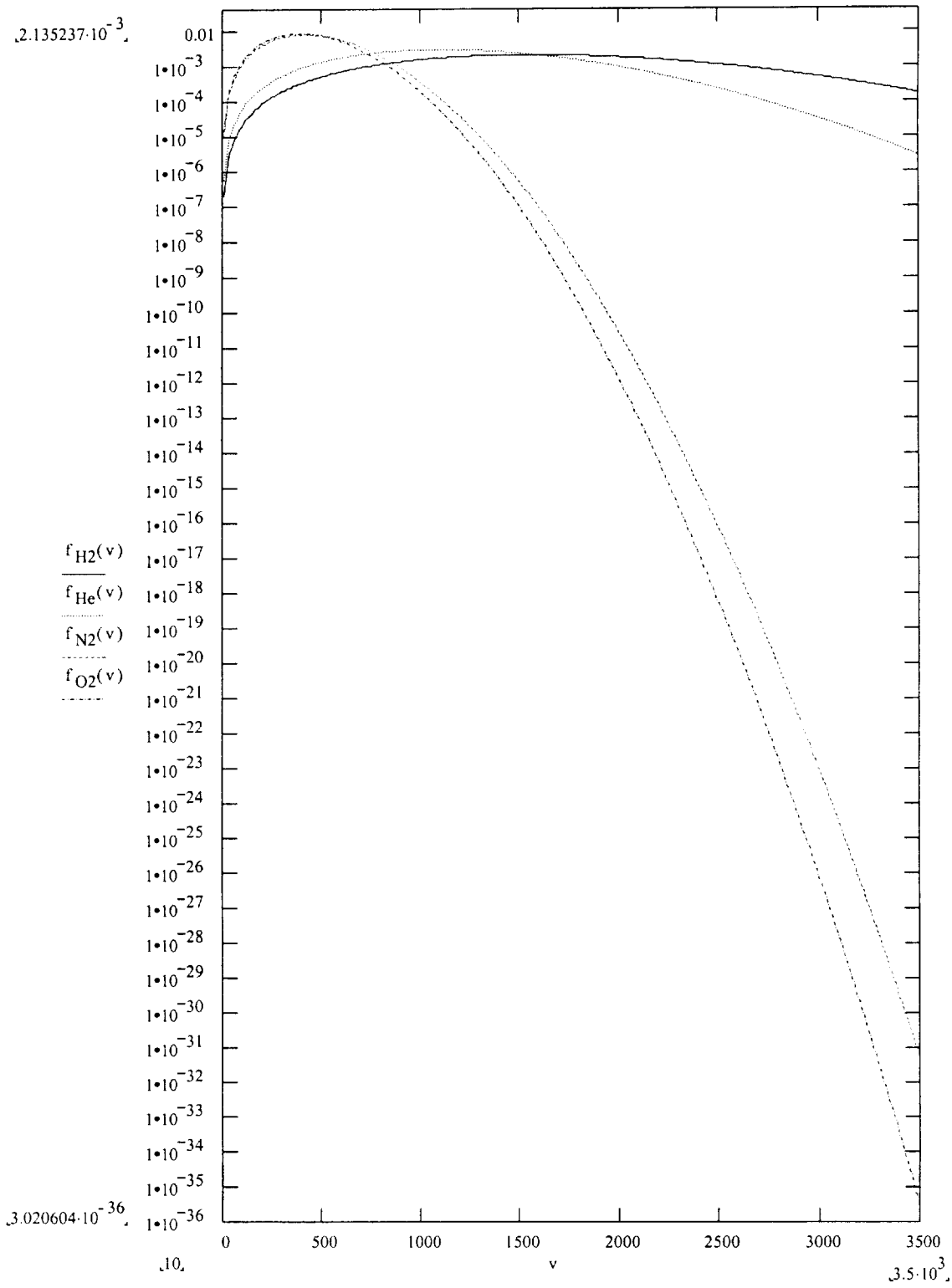

Figure 2: Distribution of speeds for H_2, He, N_2 and O_2 at 293 K

The directions of motion are isotropic; i.e. the velocities are equally distributed in all directions. The observed Doppler shift, however, is a function of the component of the velocity projected along the line of sight to the observer. The line-of-sight distribution is given by[2]:

$$f(v_x) = 4\pi\left(\frac{m}{2\pi kT}\right)^{\frac{1}{2}} e^{\frac{-mv_x^2}{2kT}}$$

where $f(v_x)$ is the probability density (i.e. $f(v_x)\ \delta v_x$ is the fraction of molecules with velocity between v_x and $v_x+\delta v_x$), m is the mass of the molecule, k is the Stephan-Boltzmann constant, and T is the absolute temperature. The distribution of line-of-sight velocities for H_2, He, N_2 and O_2 at 293 K (room temperature) are shown in Figure 3.

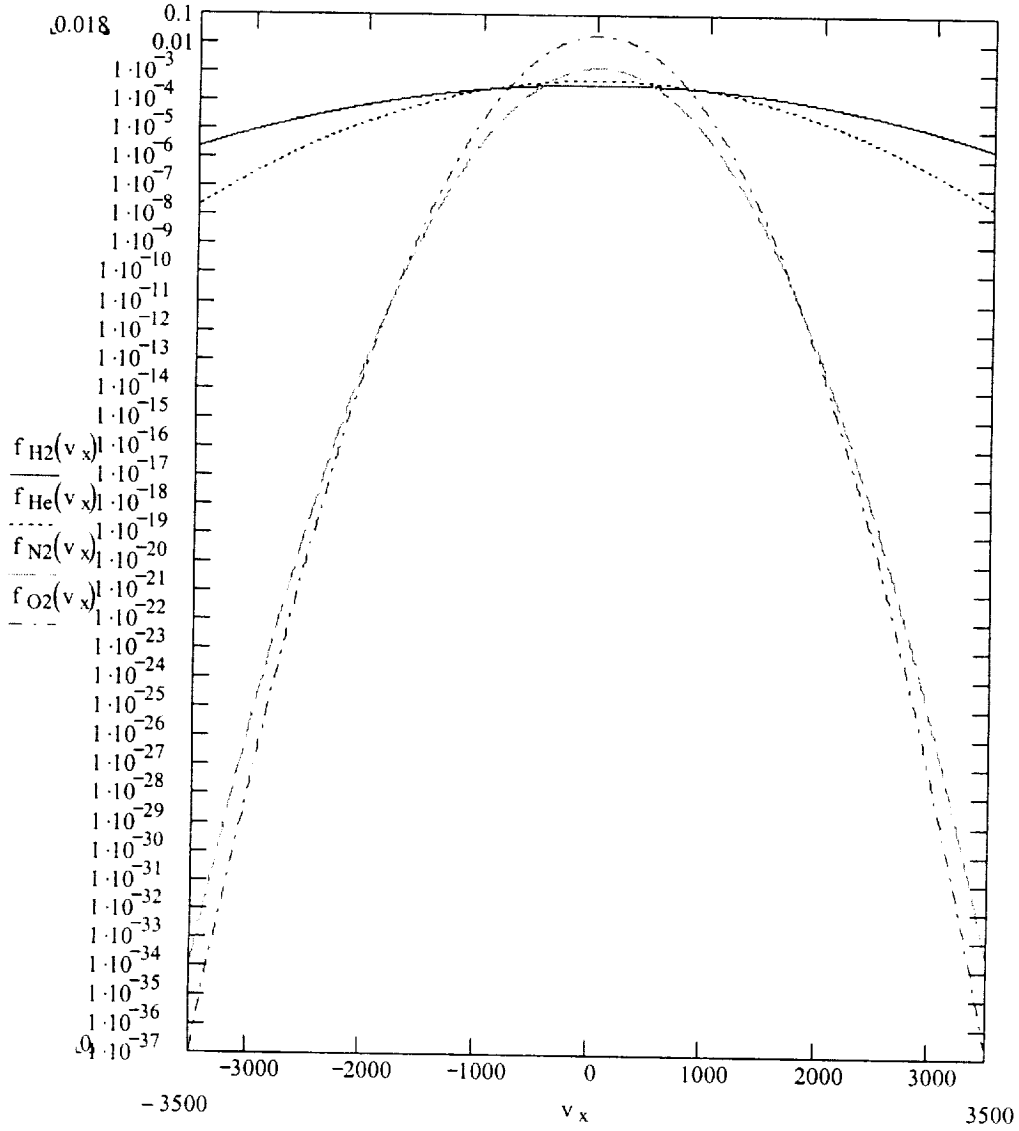

Figure 3: Distribution of line-of-sight velocities for H_2, He, N_2 and O_2 at 293 K

We have modified the equation given by Measures[2] to model backscatter from a moving target and to normalize the frequency distribution to the source frequency. The resulting distribution of Doppler shifts for backscattered light is given by:

$$g'(\Delta\omega') = \frac{1}{2\beta'\pi^{1/2}} \cdot e^{\frac{-(\Delta\omega')^2}{4\beta'^2}}$$

where $g'(\Delta\omega')$ is the probability density as a function of the relative frequency shift $\Delta\omega'$, and β' is defined as:

$$\beta' \equiv \left(\frac{2kT}{mc^2}\right)^{\frac{1}{2}}$$

This function is graphed in Figure 4 for H_2, He, N_2 and O_2 :

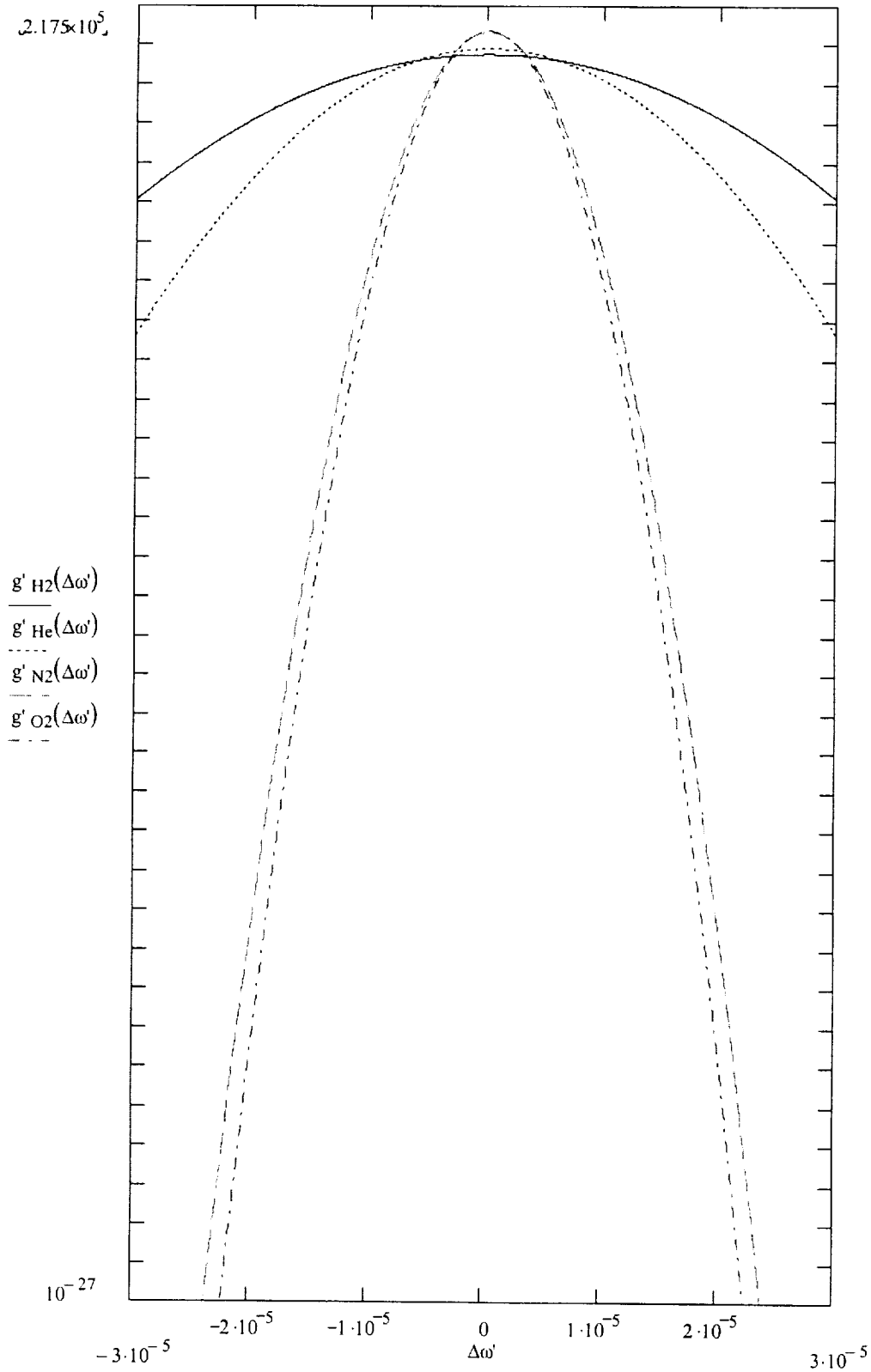

Figure 4: Probability density as a function of relative frequency shift, for H_2, He, N_2 and O_2 at 293 K

The four largest constituents of standard air[3] are shown in Table 2:

Table 2: Molar fractions for standard air

Constituent	Molar Fraction
N_2	0.78084
O_2	0.20946
Ar	0.00934
CO_2	0.00033

Together, O_2 and N_2 make up a molar fraction of 0.9903 so in the model we have neglected the Ar, CO_2, and other minor constituents. The molar fractions of H_2 or He are inputs to the model, and the molar fractions of N_2 and O_2 in the resulting mixture are given by:

$$N_2 = 0.78084 \cdot (1 - H_2 - He) \qquad O_2 = 0.20946 \cdot (1 - H_2 - He)$$

where N_2, O_2, H_2 and He are the molar fractions of the respective gasses.

The molecular densities are given by:

$$N_{H2} = N_{air} H_2 \qquad N_{He} = N_{air} He \qquad N_{N2} = N_{air} N_2 \qquad N_{O2} = N_{air} O_2$$

where $N_{air} = 2.55 \times 10^{19}$ cm^{-3} is the molecular density of air at standard temperature and pressure.

The Rayleigh cross-section for a wavelength of 694.3 nm are listed in Table 3:

Table 3: Rayleigh cross-sections

Constituent	Rayleigh Cross-section [cm^2 sr^{-1}]
N_2	2.14×10^{-28}
O_2	1.80×10^{-28}
H_2	0.44×10^{-28}
He	0.03×10^{-28}

The system design parameters are inputs to the model. These include the length of the test chamber R, and the transmitter design parameters:

- wavelength of the laser λ
- power of the laser ϕ_0
- bandwidth of the laser B

The Rayleigh cross-sections at the laser wavelength are given by:

$$\sigma = \sigma_{694.3}\left(\frac{694.3nm}{\lambda}\right)^4$$

where σ is the cross-section at wavelength λ and $\sigma_{694.3}$ is the cross-section at 694.3 nm.

Since the laser wavelength is now defined, the Doppler broadening can be expressed in rad/s rather than as a normalized frequency shift. As an example, the modeled probability densities for a laser wavelength of 532.225 nm are shown in Figure 5:

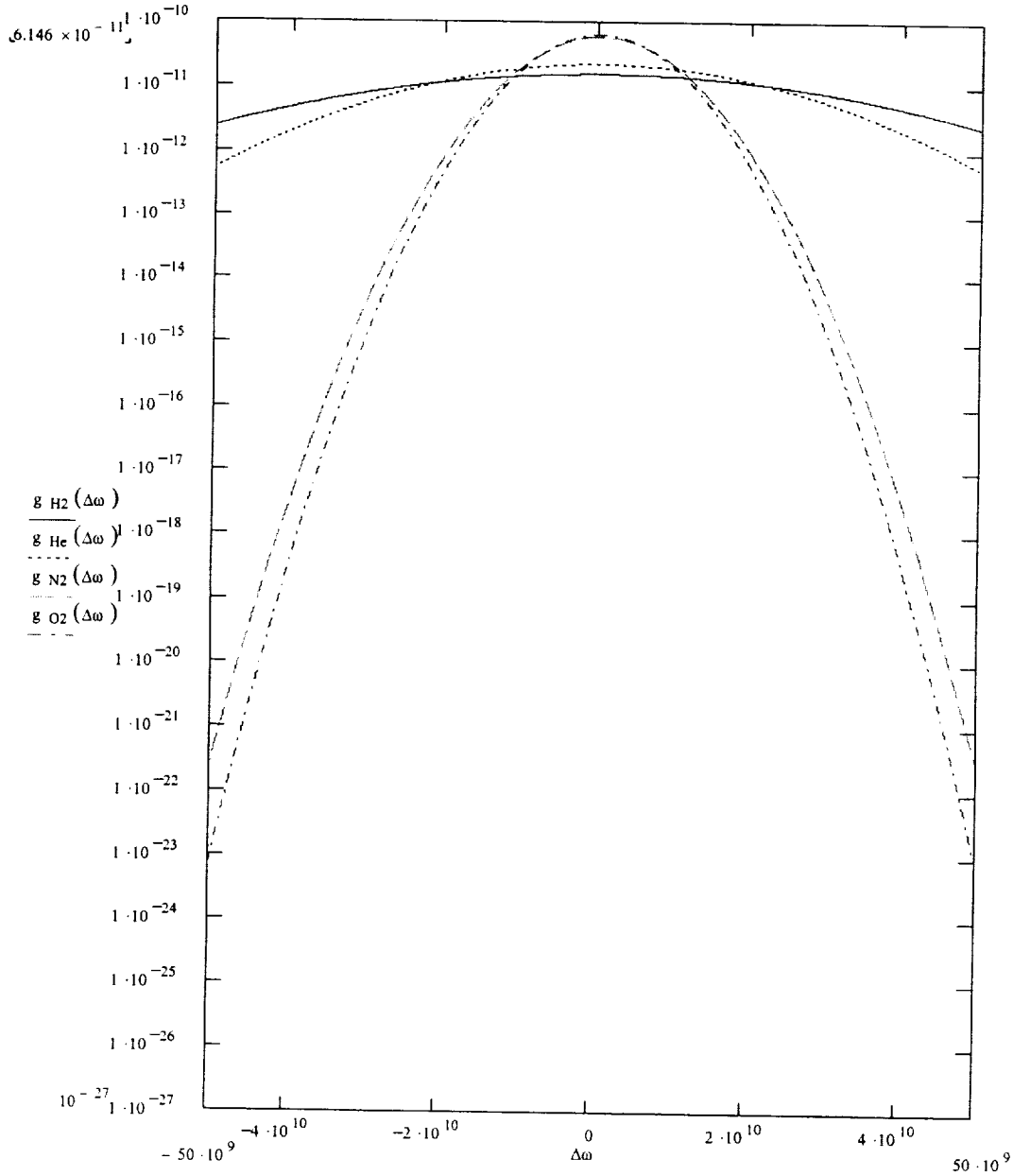

Figure 5: Probability density as a function of angular frequency shift [radians/s], for a laser wavelength of 532.225 nm, for H_2, He, N_2 and O_2 at 293 K

The spectral profile of the laser is assumed to be Gaussian, represented by a probability density of:

$$g_{laser}(\Delta\omega) = \frac{1}{B} \cdot e^{-\pi\left(\frac{\Delta\omega}{B}\right)^2}$$

where $g_{laser}(\Delta\omega)$ is the probability density as a function of the angular frequency shift $\Delta\omega$, and B is the bandwidth of the laser (in angular frequency).

The receiver design is described by the following inputs to the model:

- diameter of the collecting lens D_r
- saturation limit for the detector ϕ_{sat}
- responsivity of the detector *Resp*
- noise-equivalent-power for the detector *NEP*
- sampling time τ

The model assumes that the field-of-view of the receiver encompasses the entire illuminated volume of air. It is up to the user to select a design that does not violate this assumption.

The collected spectral flux from each constituent is given by:

$$\phi_\lambda(\Delta\omega) = \phi_0 N \sigma R \Omega_r g(\Delta\omega)$$

where $\phi_\lambda(\Delta\omega)$ is the collected spectral flux in watt· seconds [W·s], ϕ_0 is the laser flux in watts [W], N is the molecular density of the constituent in molecules per cubic centimeter [cm^{-3}], σ is the Rayleigh cross-section in square centimeters per steradian [cm^2/sr], Ω_r is the solid angle subtended by the receiver lens in steradians [sr], R is the length of the scattering volume in centimeters [cm], and $g(\Delta\omega)$ is the probability density function in units of seconds [s]. Note that the spectral units used here are in terms of angular frequency, so the spectral flux and the probability densities are *per unit angular frequency*.

Most of the laser flux will not be scattered by the gas mixture, but will instead continue to propagate until it hits a solid surface, from which it will be reflected. We have assumed that the point where the beam intersects the surface will be in the field-of-view of the receiver. The surface is modeled as a Lambertian (diffuse) reflector with unit reflectance, resulting in a spectral flux of:

$$\phi_{\lambda w}(\Delta\omega) = \phi_0 \frac{1}{\pi} \Omega_r g_{laser}(\Delta\omega)$$

where $\phi_{\lambda w}(\Delta\omega)$ is the collected spectral flux in watt· seconds [W·s], ϕ_0 is the laser flux in

watts [W], Ω_r is the solid angle subtended by the receiver lens in steradians [sr], and $g_{laser}(\Delta\omega)$ is the probability density function of the laser in units of seconds [s].

The solid angle subtended by the receiver is given approximately by:

$$\Omega_r = \frac{\frac{\pi}{4} D_r^2}{R^2}$$

The total spectral flux is the sum of the fluxes from the constituents and from the wall:

$$\phi_\lambda(\Delta\omega) = \phi_{\lambda H2}(\Delta\omega) + \phi_{\lambda He}(\Delta\omega) + \phi_{\lambda N2}(\Delta\omega) + \phi_{\lambda O2}(\Delta\omega) + \phi_{\lambda w}(\Delta\omega)$$

The predicted spectral fluxes are plotted on a logarithmic scale in Figure 6:

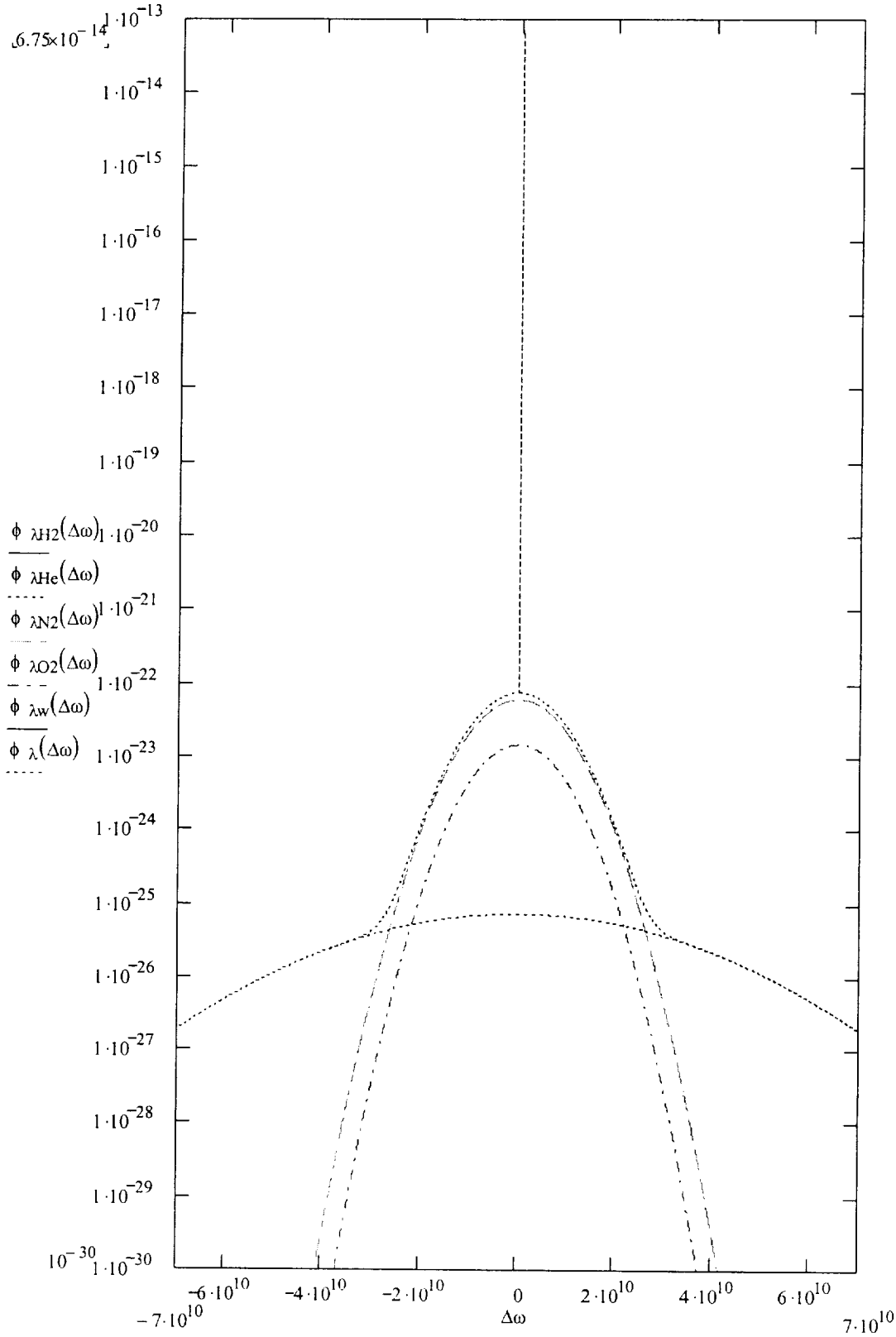

Figure 6: Predicted spectral fluxes [W·s] as a function of angular frequency shift [rad/s] for 20% He [molar fraction] at 293 K

Two detection techniques are included in the model: homodyne and direct detection. For homodyne detection the received flux is mixed with a local oscillator (flux picked off of the transmit beam) to provide amplification. The practical limit for the local oscillator flux is determined by the saturation limit of the detector. We have (arbitrarily) set the local oscillator flux to:

$$\phi_{LO} = 0.9 \cdot \phi_{sat}$$

where ϕ_{sat} is the saturation limit of the detector in Watts, and ϕ_{LO} is the selected flux for the local oscillator in watts. As may be seen from Figure 6, most of the signal at the high frequencies results from the He in this example. A spectrum analyzer or electronic filters may be used to select the signal from the frequency range of interest, which in this example is 30 – 60 GHz. The flux within this frequency band is given by:

$$\phi_{band} = \int_{-\omega_{\max}}^{-\omega_{\min}} \phi_\lambda(\omega) d\omega + \int_{\omega_{\min}}^{\omega_{\max}} \phi_\lambda(\omega) d\omega$$

where ϕ_{band} is the in-band flux, $\phi_\lambda(\omega)$ is the collected spectral flux, and ω_{min} and ω_{max} are the limits of the desired band.

The homodyned signal is given by:

$$S = Resp\sqrt{\phi_{band}\phi_{LO}}$$

where S is the signal in amps, and $Resp$ is the responsivity of the detector in amps/watt.

The detector noise is given by:

$$N_{\det} = Resp \cdot NEP\sqrt{\frac{1}{\tau}}$$

where N_{det} is the detector noise in amps, NEP is the noise equivalent power of the detector in amps/(Hz)$^{1/2}$ and τ is the sampling time in seconds.

The shot noise (also called photon noise or quantum noise) is a function of the signal, given by:

$$\phi = \phi_{LO} + \int_{-\infty}^{\infty} \phi_{\lambda}(\Delta\omega) d\Delta\omega$$

$$\phi' = \phi \frac{\lambda}{hc}$$

$$N'_{shot} = \sqrt{\phi'}$$

$$N_{shot} = Resp \cdot N'_{shot} \frac{hc}{\lambda} \sqrt{\frac{1}{\tau}}$$

where ϕ is the total flux in watts, h is Planck's constant, c is the speed of light, ϕ' is the flux in photons/s, N'_{shot} is the shot noise in photons, and N_{shot} is the shot noise in amps.

Finally, the signal-to-noise ratio (SNR) for homodyne detection is given by:

$$SNR = \frac{S}{\sqrt{N_{det}^2 + N_{shot}^2}}$$

In the direct detection approach, we would use a vapor absorption filter to suppress the flux that is reflected from the wall. The absorption line is assumed to have a Gaussian profile, modeled as:

$$OD(\Delta\omega) = OD_{\max} \cdot e^{-\pi\left(\frac{\Delta\omega}{B_f}\right)^2}$$

where $OD(\Delta\omega)$ is the optical depth (exponential absorption coefficient) at a frequency difference of $\Delta\omega$ from the center of the absorption line in rad/s, and B_f is the bandwidth of the absorption line in rad/s. The transmittance profile is then given by:

$$t(\Delta\omega) = 10^{OD(\Delta\omega+\varepsilon)}$$

where $t(\Delta\omega)$ is the transmittance as a function of frequency difference relative to the laser frequency, and ε is the offset (error) between the center of the spectrum of the laser and the center of the spectrum of the absorption line in rad/s.

When using a vapor absorption filter, all of the fluxes will be attenuated by the transmittance function of the filter:

$$\phi_\lambda(\Delta\omega) = t(\Delta\omega)\phi_0 N\sigma R\Omega_r g(\Delta\omega)$$

$$\phi_{\lambda w}(\Delta\omega) = t(\Delta\omega)\phi_0 \frac{1}{\pi}\Omega_r g_{laser}(\Delta\omega)$$

and the total flux is again given by:

$$\phi_\lambda(\Delta\omega) = \phi_{\lambda H2}(\Delta\omega) + \phi_{\lambda He}(\Delta\omega) + \phi_{\lambda N2}(\Delta\omega) + \phi_{\lambda O2}(\Delta\omega) + \phi_{\lambda w}(\Delta\omega)$$

The predicted fluxes are plotted in , using an example absorption line from an iodine vapor absorption cell:

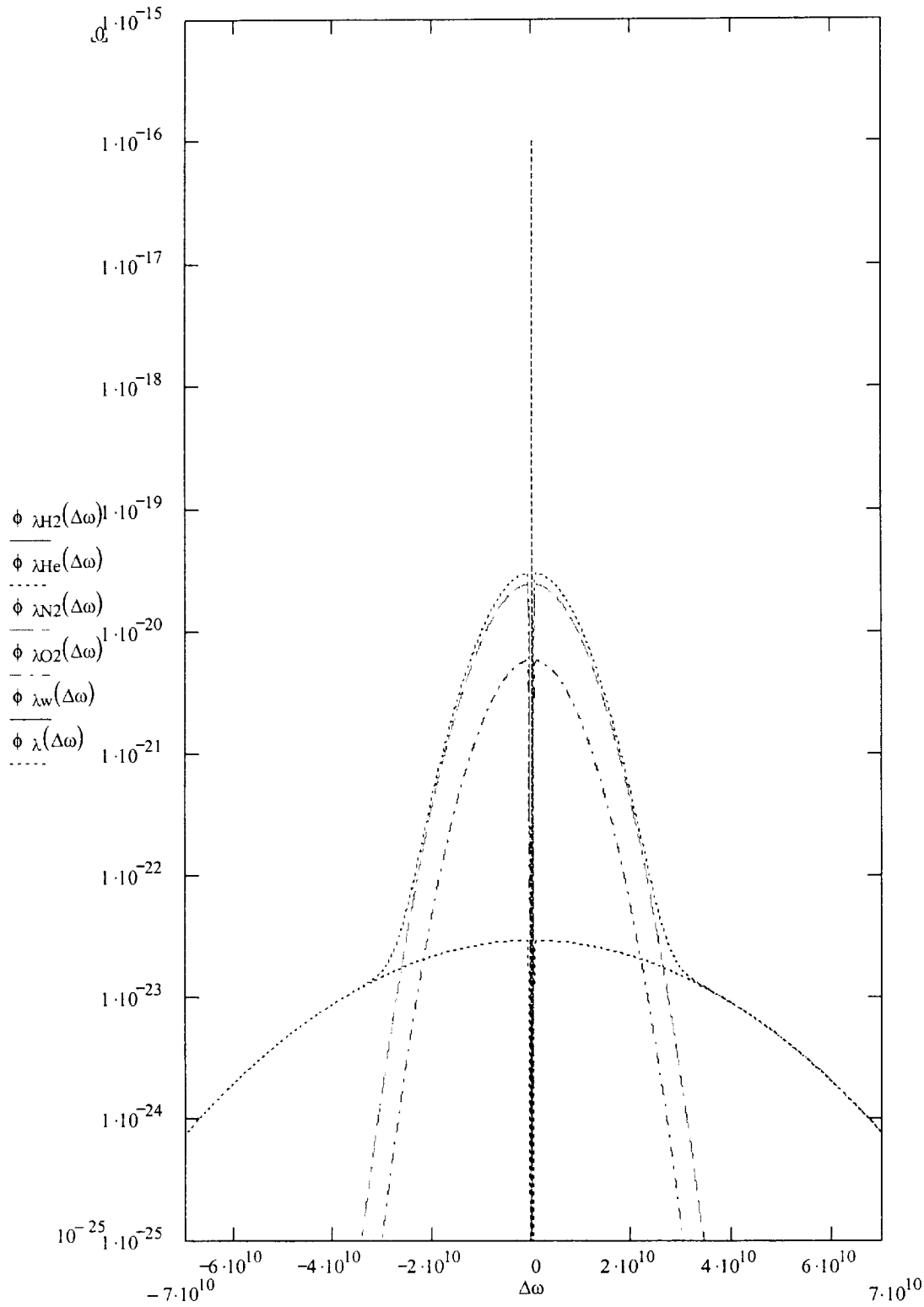

Figure 7: Predicted spectral fluxes [W·s] as a function of angular frequency shift [rad/s] for 20% He [molar fraction] at 293 K, using an iodine absorption line with OD_{max} = 6, $B_f = 5.6 \cdot 10^8$, and ε = 100 MHz,

For direct detection, the in band flux is simply:

$$\phi_{band} = \int_{\omega_{\min}}^{\omega_{\max}} \phi_{\lambda}(\Delta\omega) d\Delta\omega$$

and the signal is simply:

$$S = Resp \cdot \phi_{band}$$

The detector noise, shot noise and SNR remain the same as for homodyne detection.

3 PLAN TO ADVANCE RAYLEIGH DOPPLER TECHNIQUE FROM TRL 2 TO TRL 3

3.1 Conceptual Designs

We have considered three basic approaches to implementing a Rayleigh Doppler technique. These differ in the techniques used to discriminate between frequencies and the techniques used to detect the signal. The first of these approaches has three variations, resulting in five individual techniques:

1) Heterodyne
   a) Homodyne
   b) Offset Homodyne
   c) Heterodyne
2) Vapor Absorption Filter
3) Fabry Perot

These techniques are not mutually exclusive; they may be used in combination, thus providing a large number of potential conceptual designs to be considered.

The heterodyne approach uses a local oscillator (a laser) to both amplify the signal on the detector and shift the frequency from optical frequencies (which are ~100's of THz) down to 10's of GHz. The amplification is proportional to the square root of the local oscillator flux, but the local oscillator flux must be limited to below the saturation limit of the detector.

The heterodyne family of approaches is subdivided into three variations: *homodyne*, *offset homodyne,* and *heterodyne*. In the homodyne variation, the local oscillator is extracted from the transmit beam using a pick-off mirror. The frequencies of the homodyne signal are then equal to the difference between the transmit frequency and the received frequencies. In order to respond to these frequencies, the detector must have a bandwidth of 10's of GHz.

For offset homodyne, the local oscillator is also picked off from the transmit laser, but the transmitted beam is frequency shifted by an electro-optic modulator (EOM) at a point after the pick-off mirror but before the beam enters the test cell. The offset would in principle be chosen to be close to the frequencies of interest, thus reducing the bandwidth required for the detector, but this variation requires a high-frequency EOM.

For a true heterodyne approach, two separate lasers are used: one for the transmitter, and the other for the local oscillator. This allows the center frequency to be offset without the need for an EOM, but it requires two lasers, both of which must be highly stable in frequency, and one of which must be tunable in frequency.

3.2 Technology Surveys

The feasibility and affordability of any of these techniques depends upon the technologies that are currently available, particularly in regards to lasers, modulators, detectors, filters, and frequency discriminators.

3.2.1 Laser Technologies

The technology map for the laser, summarized in Table 4, shows the trade space in dimensions of wavelength, power, linewidth, cost and weight. The received flux depends upon the transmitted flux and the Rayleigh cross-section. The cross-section in turn depends upon the laser wavelength. So we have defined a merit function as:

$$Merit \equiv \frac{\phi_0}{\lambda^4}$$

where ϕ_0 is the optical power of the laser, and λ is the wavelength of the laser.

Table 4: Laser technology survey

Wavelength nm	Power mW	Merit power/wave^4	Linewidth MHz	Cost	Weight kg	Model
244	100	28.2	< 5	$63,000	93	Innova 90C FreD
244	125	35.3	< 5		93	Innova 300C FreD
257	1000	229.2	< 5		304	Innova Sabre FreD
266	200	39.9		$100,000	59	Azure 266
266	200	39.9	10			MBD-266
488	20	0.4	< 5	$16,000	2	Sapphire 488
488	1000	17.6	< 5		81	Innova 90C-A3
514	1400	20.1	< 5	$35,000	81	Innova 90C-A3
488	1800	31.7	< 5		81	Innova 90C-A6
514	2400	34.4	< 5		81	Innova 90C-A6
488	750	13.2	< 5	>$50,000	81	Innova 300C-I304
514	1000	14.3	< 5		81	Innova 300C-I304
488	1400	24.7	< 5		81	Innova 300C-I308
514	1900	27.2	< 5		81	Innova 300C-I308
532	2000	25.0	5	$40,000	43	Verdi Compass-V2
532	10000	124.8	5		51	Verdi Compass-V10
532	15	0.2	< 5		2	Compass 214M
532	20	0.2	< 5	$12,000		Compass 315M-20
532	150	1.9	< 5	$23,000	7	Compass 315M-150

3.2.2 *Detector technologies*

The detector technology map is shown in Table 5, and illustrated graphically in Figure 8:

Table 5: Detector technology survey

Product	Response (nm)	NEP (W/sqr(Hz))	Dark Current (nA)	Bandwidth	Responsivity	Diameter	Saturation	Price ($)	Manufacturer
UV Enhanced PIN Photodiodes	200 - 1050	1.9*10^-13 - 8.9*10^-14	4.4 - 30	<33 MHz	>0.10 A/W	3.8 - 10 mm	1.5 - 10 mW		Advanced Photonix
PIN Photodiode	254	6.0*10^-12	6	22 MHz					Advanced Photonix
Non-Cooled Avalanche Photodiode	150 - 900	1.6*10^-13 - 5.50*10^-14		0.2 - 14 MHz					Advanced Photonix
Solar Blind Schottky AlGaN	200 - 280		1 - 1000	0.1 - 2 MHz				50 - 800	APA Optics
GaAs Photodiode	175 - 350							425 - 650	International Light
High Gain Detector	185 - 320								International Light
Germicidal Detector (PMA2122)	249 - 261							600	Solar Light
SiC UV Photodiode	200 - 350		<0.000005	<100 MHz				55 - 166	Boston Electronics
SiC UV Detector	240 - 400		0.01	200 kHz					Laser Components
General Research Detector (D-15)	400 - 1700	9.0*10^-11	50	30 GHz				4800	Newport
High-Speed Detector (PX-D7)	400 - 900	3.6*10^-10	10	60 GHz	1.7 V/W @ 670 nm ~1.4 V/W @ 532 nm	50 um fiber	1 mW	6400	Newport

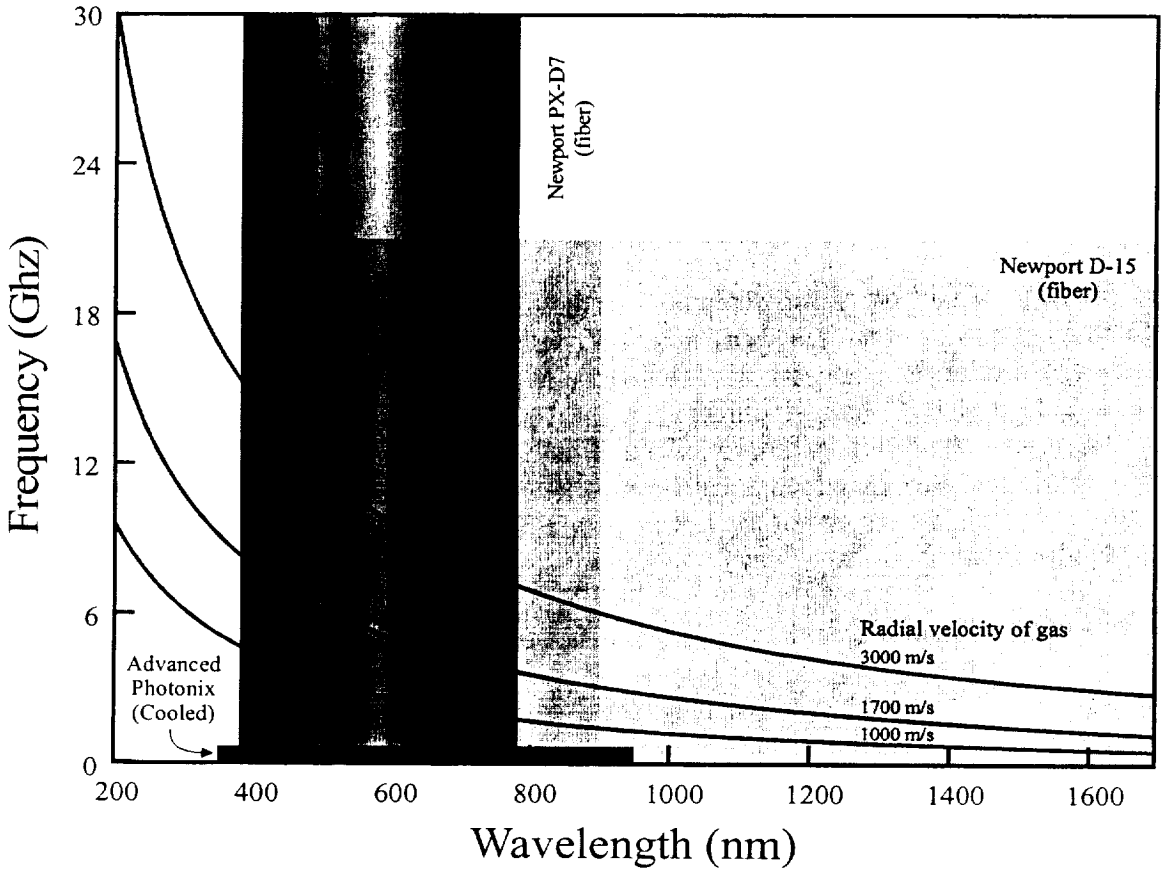

Figure 8: Detector technology map

3.2.3 *Modulator technologies*

No modulators were found that could provide the required frequency shift of 10's of GHz.

3.2.4 *Vapor filter technologies*

Only one commercial source was found for vapor absorption filters. Innovative Scientific Solutions Incorporated sells sealed iodine molecular vapor absorption filter cells with prices starting at ~ $ 2 K. No commercial sources were found for mercury atomic absorption filter cells, but some researchers are open to the idea of providing one to order.

3.2.5 *Frequency discrimination technologies*

Heterodyne techniques shift the frequencies down to 10's of GHz, a range for which electronic spectrum analyzers are widely available. For the direct detection technique a tunable vapor filter, tunable laser, or a Fabry-Perot etalon could provide frequency-scanning capability. Frequency tunability for lasers is feasible but expensive. Frequency-tunability for vapor filters is affordable, but very slow and limited in range. Fabry-Perot etalons designed for determining the spectral profiles of lasers are commercially available and affordable.

3.3 Conceptual Designs

The technology maps have provided information that constrains the design options:

The primary driver for laser selection is the cost. The primary trade-off in laser technology is price versus the merit function (based on power and wavelength). Higher powers and shorter wavelengths drive the cost upwards. Only a few of the lasers in Table 4 fit within projected budget constraints for Phase 3. The heterodyne technique is therefore a poor candidate for Phase 3 since it requires two lasers, both of which must be highly stable and one of which must be tunable. The ultraviolet lasers are outside the budget constraints; as are all but the lowest power blue lasers, so green wavelengths seem optimum for Phase 3.

The lack of suitable modulators implies that offset homodyne is not currently feasible.

Detectors are not a cost driver but they are a key performance driver. Two classes of detectors are available: those with high bandwidth but very small sensitive area, and those with moderate bandwidth and relatively large area. The former are appropriate for the heterodyne family of techniques, and the latter for direct detection.

Iodine vapor cells are appropriate for use at green wavelengths, commercially available, and affordable. Such a filter could provide substantial reduction in the background from flux reflected from the wall, so there seems worthwhile to include one in an experiment. The theoretical model (see section 2) shows that the width of the iodine absorption lines

is too narrow to block the unwanted signal from the O2 and N2. The survey of frequency discrimination technologies (see section 3.2.5) shows that a Fabry-Perot etalon would be appropriate for Phase 3.

Thus, based on the technology surveys, the design options for a Phase 3 experiment were narrowed down to two conceptual designs:

1) *Homodyne*, at a *green* wavelength, with a *fast* detector; and,
2) *Direct detection,* at a *green* wavelength, with a *large-area* detector, an *iodine absorption cell,* and a *Fabry-Perot etalon.*

3.4 Predicted Signal-to-Noise Ratios

While the technology surveys constrained the feasible approaches, it was also necessary to determine whether the SNR's are expected to be sufficient to be used to validate the theoretical model and prove the principle of the Rayleigh Doppler technique. This section present the results of four designs evaluated using the model developed in section 2. Designs 1a and 1b both use homodyne detection while designs 2 and 3 are based on direct detection incorporating vapor absorption filters. Designs 1a and 2 fit within the budget constraints for Phase 3, while designs 1b and 3 illustrate what would be possible in a future phase, employing currently available lasers. These results are summarized in Table 6:

Table 6: Summary of four designs

	#1a	#1b	#2	#3
Target:				
Concentration	20% He	20% He	20% He	20% He
Range	1 m	1 m	1 m	1 m
Laser:	Compass 315M-150	Verdi V10	Compass 315M-150	Azure 266
Wavelength	532 nm	532 nm	532 nm	266 nm
Power	150 mW	10000 mW	150 mW	200 mW
Bandwidth	< 1 MHz	< 1 MHz	< 1 MHz	< MHz
Wavelength stability	100 MHz	100 MHz	100 MHz	MHz
Receiver:				
Technique	**Homodyne**	**Homodyne**	**Iodine Filter + Fabry-Perot**	**Mercury Filter + Fabry-Perot**
Diameter	0.3 cm	0.3 cm	6 cm	6 cm
Sampling frequency	1 Hz	1 Hz	1 Hz	1 Hz
Detector:	Newport PXD-7	Newport PXD-7	Photonix SD041-12-22-011	Photonix SD172-13-23-222
NEP	3.6×10^{-10} W/(Hz)$^{1/2}$	3.6×10^{-10} W/(Hz)$^{1/2}$	1.7×10^{-14} W/(Hz)$^{1/2}$	$7. \times 10^{-14}$ W/(Hz)$^{1/2}$
Responsivity	1.4 A/W	1.4 A/W	0.20 A/W	0.10 A/W
Dimensions	50 μm dia. fiber	50 μm dia. fiber	1000 x 833 μm	4700 x 3800 μm
Saturation	1 mW	1 mW		
Bandwidth	60 GHz	60 GHz	0.1 GHz	0.017 GHz
Spectral range	400-900 nm	400-900 nm		
Signal-to-Noise:				
Signal	1.4×10^{-9} A	11×10^{-9} A	4×10^{-14} A	2×10^{-12} A
Detector noise	5×10^{-10} A	5×10^{-10} A	3×10^{-15} A	7×10^{-15} A
Photon noise	3×10^{-11} A	3×10^{-11} A	0 A	0 A
SNR	**3**	**20**	**10**	**300**

3.5 Experiment Design

Advancement of the Rayleigh Doppler technique from TRL 2 to TRL 3 requires a proof-of-concept experiment. The objectives of this experiment would be to validate the theoretical model and to demonstrate the principle of operation for this technique. As shown in Table 6, the predicted SNR's are reasonable for both the homodyne and the direct detection approaches. Since the cost of the detectors and iodine vapor cell are a relatively small part of the budget, we recommend experimentation with both approaches.

It is important to note that the minimum detectable concentration for this technique is limited by *sensitivity*, while all the other techniques for He are limited by *clutter*. The other techniques all ultimately measure *density*, which is affected by temperature variations. Therefore we expect that technological improvements in sensitivity will improve the performance achievable with this technique, but will not improve the performance of any other technique applicable to He.

In both experiments the plan is to vary the concentration of He in the test cell and measure the signal. A beam dump may be used initially to minimize the background flux, followed by backgrounds that are representative of the intended operational environment. Other parameters such as the frequency range, FOV, local oscillator flux, etc., may be varied in order to validate the theoretical model.

3.5.1 Homodyne experiment

The small area of the high-bandwidth detector required for the homodyne approach severely limits the field-of-view (FOV) of the receiver. A monostatic configuration must therefore be used to enable this narrow FOV to encompass the volume illuminated by the laser. In a monostatic configuration, the transmitter and receiver use the same aperture. Isolation of the transmitted flux from the receiver is achieved by the use of a quarter wave plate and polarization beamsplitter. This configuration is illustrated in Figure 9 and the required parts are listed in Table 7.

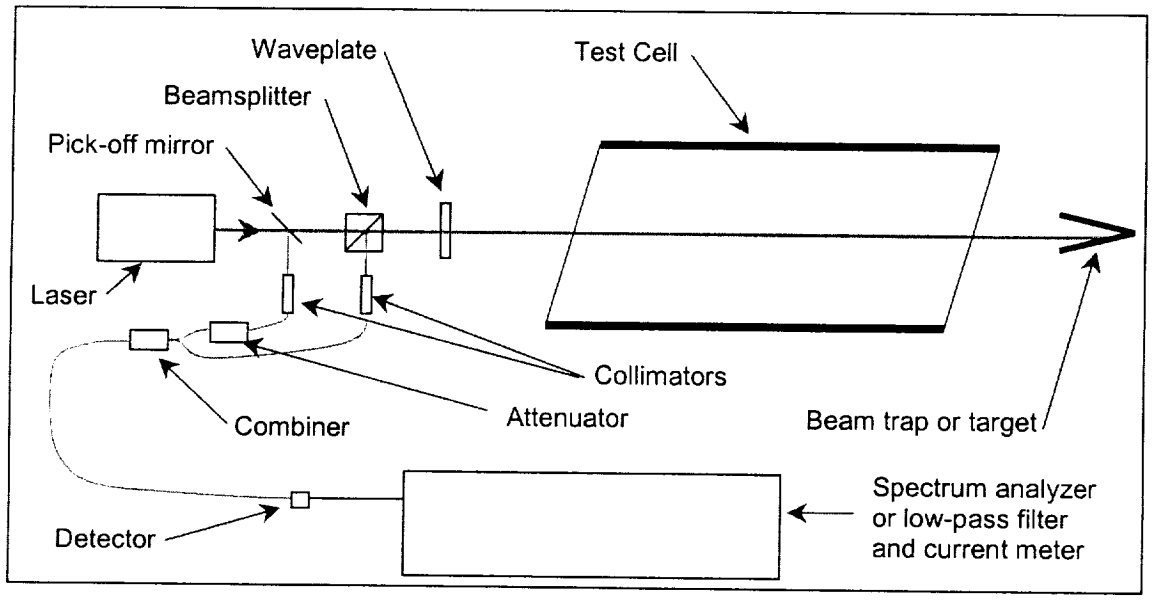

Figure 9: Homodyne experiment

3.5.2 *Direct detection experiment*

The large-area detectors available for the direct detection approach allow the use of a bistatic configuration, in which the receiver aperture is separate from the transmitter aperture. This allows the use of a relatively large receiver aperture. This configuration is illustrated in Figure 10 and the required parts are listed in Table 7.

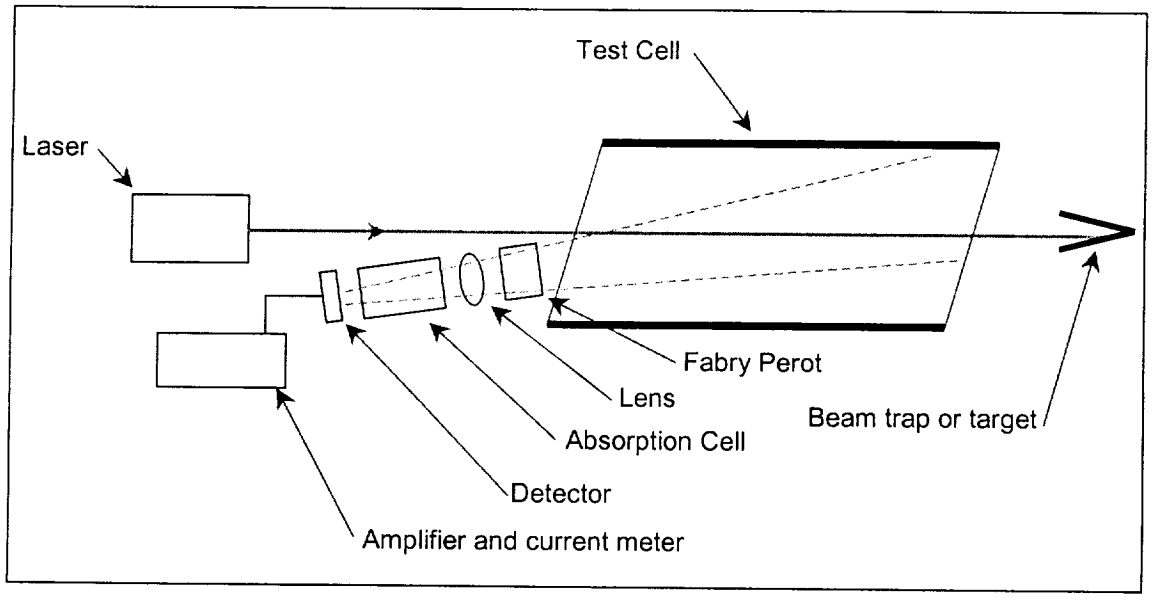

Figure 10: Direct detection experiment

Table 7: Parts list

Part	Mfr.	Mfr. Part No.	Cost
Laser	Coherent	Compass 315M-150	23,000
Beamsplitter	Newport	10BC16PC.3	350
Waveplate	Newport	10RP14-16	495
Collimators (2)	Oz Optics	HPUCO-35-532-M-0-2.7AS	600
Attenuator	Oz Optics	BB-200-55-532-M	100
Combiner	Oz Optics	FUSED-12-532-a/b-50/50-555-3-0.5	500
Fiber cables	Oz Optics	N/A	100
Fabry-Perot	Coherent	33-6446	4,566
Lens	Newport	KPA052-C	67
Iodine cell	ISSI	N/A	3,000
Detector, fast	Newport	PXD-7	6,372
Detector, large-area	Photonix	SD041-12-22-011	100
Amplifier	<TBD>	<TBD>	<TBD>
Current meter	<TBD>	<TBD>	<TBD>
Low-pass filter	<TBD>	<TBD>	<TBD>
Mount, laser	Newport	MRP4-1 (6)	354
Mount, beamsplitter	New Focus	9481	295
Mount, waveplate	New Focus	9401	150
Mount, collimator (2)	New Focus	9872-K	398
Mount, lens	Newport	AC-2	48
Test cell	<TBD>	<TBD>	<TBD>

4 IDENTIFY RESEARCHERS AND RESOURCES FOR FURTHER ADVANCEMENT

4.1 Lidar and Rayleigh Scattering

4.1.1 Dr. Richard Seasholtz

Glenn Research Center

4.1.2 Dr. Richard B. Miles

Professor of **Mechanical and Aerospace Engineering (MAE)**, School of Engineering and Applied Science (SEAS), **Princeton University**.

- Email address: **miles@princeton.edu**
- Office phone: **609-258-5131**
- Departmental fax phone: **609-258-1139**
- Regular mail address:

D414 Engineering Quad,
Princeton University, Princeton, NJ 08544

Research Interests

Research interests include the development of new laser-based capabilities for quantitative imaging of flow fields and combustion phenomena. Other research includes laser-based diagnostics such as pollution monitoring and optical air data systems for high-speed aircraft. This work involves the use of nonlinear optics and precision laser spectroscopy together with the development of new laser sources. Some examples of recent work are:

- the development of a new capability for writing lines and patterns into air in order to track air motion;
- imaging of time-evolving supersonic structure by Rayleigh scattering;
- measurement of high-speed velocity, temperature and density fields by Filtered Rayleigh Scattering;
- two-photon, laser-induced fluorescence imaging of molecular hydrogen;
- the capability of writing lines and patterns into water.
- the possibility of using high power electron beams and lasers as drivers for hypersonic ground test facilities.
- the use of plasmas for high speed air control and electromagnetic protection.

Curricula Vita

PROFESSIONAL BACKGROUND
1982- Professor, Dept. of Mechanical & Aerospace Engineering, Princeton University
1994-2000 Director of Graduate Studies, Dept. of Mechanical & Aerospace Eng., Princeton Univ.
1980-1996 Chairman, Engineering Physics Program, Princeton University
1978-1982 Associate Professor, Dept. of Mechanical & Aerospace Engineering, Princeton Univ.
1972-1978 Assistant Professor, Dept. of Mechanical & Aerospace Engineering, Princeton Univ.
Summer 1972 Research Associate, Department of Electrical Engineering, Stanford University

EDUCATION

1972 Ph.D. Stanford University, Electrical Engineering
1967 M.S. Stanford University, Electrical Engineering
1966 B.S. Stanford University, Electrical Engineering

PROFESSIONAL SOCIETIES

American Institute of Aeronautics and Astronautics, Fellow
Optical Society of America, Fellow
Institute of Electrical and Electronic Engineers, Senior Member
American Physical Society, Member

PROFESSIONAL ACTIVITIES

Member, Board of Directors, Fannie & John Hertz Foundation
Executive Committee, Princeton Univ., Photonics & Opto-Electronics Center
Member, NASA New Millenium Interferometer Project Independent Assessment Team
Chairman, AIAA Aerodynamic Measurement Technology Technical Committee, '92-'94
Chairman, DoE Basic Energy Sciences Combustion Diagnostics Program Review, Oct. '92
Chairman, 1986 Gordon Conference on Vibrational Spectroscopy
Member, Board of Directors, Ice Cap, Inc., Hamilton, New Jersey

(212 Refereed Conference Manuscripts and Journal Articles; 5 U.S. Patents)

Invited Lectures (2000-2001)

Mar 28, 2000 "MHD--Air Plasma Processes for Hypersonics," Briefing to the USAF Scientific Advisory Board Study Team "Why and Whither Hypersonics Research in the USAF," Arlington, VA.

Apr. 5-7, 2000 "The MARIAH II Radiatively Heated/MHD-Driven Hypersonic Wind Tunnel Concept," Second Workshop on Magneto and Plasma Aerodynamics for Aerospace Applications, Institute Of High Temperatures, Russian Academy of Sciences, Moscow, Russia.

Apr. 19, 2000 "Review of Princeton Air Plasma Ramparts MURI Program," AFOSR MURI Project Review, Columbus, OH.

Jun 19-20, 2000 "Flow Control by Energy Addition into High-Speed Air," Fluids 2000, Denver, CO.

July 18, 2000 "RDHWT/MARIAH II Program (An R&D Program for an Advanced M=8-15 Hypersonic Wind Tunnel)," Briefing to DDR&E, Washington, DC.

Aug. 19, 2000 "MARIAH II--Solution, Technology Status, and Future Plans," Briefing to Senator Conrad Burns, Butte, MT.

Sept. 6-7, 2000 "Microwave-Driven Air Plasma Studies for Drag Reduction and Power Extraction in Supersonic Air," AFOSR 2000 Contractors' Meeting in Unsteady Aerodynamics & Hypersonics, Monterey, CA.

Sept. 19-22 2000 "La Methode RELIEF de Marquage des Ecoulements et ses Applications dans L'Etude des Phenomenes de Transport et de Melange," Presented at the 7th Congres Francophone de Velocimetrie Laser, Marseille, France (Keynote Speaker).

March 8, 2001 "RDHWT/MARIAH II Program," The Ohio State University, Columbus, OH.

April 27, 2001 "Flow Field Diagnostics by Filtered Rayleigh and Raman Scattering," Georgia Tech, Atlanta, Georgia.

June 27, 2001 "Novel Trends in Nonlinear Laser Spectroscopy and Optical Diagnostics," XVII International Conference on Coherent and Nonlinear Optics (ICONO), Belarus Cultural Center, Minsk, Belarus, June 26-July 1, 2001 (Invited Keynote Speaker).

July 4, 2001 "A Renaissance in Raman Imaging Using Dispersive and Fluorescent Atomic Filers," 2001 Gordon Research Conference on Laser Diagnostics in Combustion, Mount Holyoke College, South Hadley, MA.

Publications in Refereed Journals and Review Articles (2001)

1. R.B. Miles, A. Yalin, Z. Tang, S. Zaidi, and J. Forkey, "Flow Field Imaging Through Sharp-Edged Atomic and Molecular Notch Filters," J. Measurement Science Technology Vol. 12 (2001) pp. 442-451.
2. S.O. Macheret, M.N. Shneider, and R.B. Miles, "Modeling of Discharges Generated by Electron Beams in Dense Gases: 'Fountain' and 'Thunderstorm' Regimes," Physics of Plasmas, Vol. 8, May 2001, pp. 1518-1528.
3. R.B. Miles, W. Lempert, and J. Forkey, "Laser Rayleigh Scattering," J. of Measurement Science & Technology, Vol. 12, (2001) R33-R51 Invited (Published by the Institute of Physics Publishing, Bristol, England).
4. S.O. Macheret, M.N. Shneider, and R.B. Miles, "Electron Beam Generated Plasmas in Hypersonic Magnetohydrodynamic Channels," AIAA Journal, Vol. 39, No. 6, June 2001, pp. 1127-1138.

Published Conference Proceedings (2001)

1. S. Zaide, Z. Tang, A. Yalin, P. Barker, and R. Miles, "Filtered Thomson Scattering in an Argon Plasma," Paper #AIAA-2001-0415, 39th AIAA Aerospace Sciences Meeting & Exhibit, Reno, NV, Jan. 8-11, 2001.
2. S. Macheret, M. Shneider, and R. Miles, "MHD Control of External Supersonic Flow with Electron Beam Ionization," Paper #AIAA-2001-0492, 39th AIAA Aerospace Sciences Meeting & Exhibit, Reno, NV, Jan. 8-11, 2001.
3. P. Barker, A. Meschanov, and R. Miles, "Temperature Measurements in Plasmas Using Coherent Rayleigh Scattering," Paper #AIAA-2001-0416, 39th AIAA Aerospace Sciences Meeting & Exhibit, Reno, NV, Jan. 8-11, 2001.
4. S. Macheret, M. Shneider, and R. Miles, "Potential Performance of Supersonic MHD Power Generators," Paper #AIAA-2001-0795, 39th AIAA Aerospace Sciences Meeting & Exhibit, Reno, NV, Jan. 8-11, 2001.

5. R. Miles and P. Wu, "Three-Dimensional Imaging of Hypersonic Flow at MHz Rate, "Paper #AIAA-2001-0846, 39th AIAA Aerospace Sciences Meeting & Exhibit, Reno, NV, Jan. 8-11, 2001.
6. V. Chiravalle, R. Miles, and E. Choueiri, "Numerical Simulation of Microwave Sustained Supersonic Plasmas for Application to Space Propulsion," Paper #AIAA-2001-0962, 39th AIAA Aerospace Sciences Meeting & Exhibit, Reno, NV, Jan. 8-11, 2001.
7. I.G. Girgis, G.L. Brown, R.B. Miles, and R.J. Lipinski, "Fluid Mechanics of a Mach 7-12 Electron Beam Driven, Missile-Scale, Hypersonic Wind Tunnel: Modeling and Predictions," Paper #AIAA-2001-2777, 31st AIAA Fluid Dynamics Conference & Exhibit, Anaheim, Ca, June 11-14, 2001.
8. S.O. Macheret, M.N. Shneider, and R.B. Miles, "Energy-Efficient Generation of Nonequilibrium Plasmas and their Applications to hypersonic MHD Systems," Paper AIAA-2001-2880, 32nd AIAA Plasmadynamics and Lasers Conference and 4th Weakly Ionized Gases Workshop, Anaheim, CA, June 11-14, 2001.
9. S.O. Macheret, M.N. Shneider, and R.B. Miles, "Modeling of Plasma Generation in Repetitive Ultra-short DC, Microwave, and Laser Pulses," Paper AIAA-2001-2940, 32nd AIAA Plasmadynamics and Lasers Conference and 4th Weakly Ionized Gases Workshop, Anaheim, CA, June 11-14, 2001.
10. R.B. Miles, S.O. Macheret, L. Martinelli, R. Muray, M. Shneider, Yu.Z Ionikh, J. Koine and J. Fox, "Plasma Control of Shock Waves in Aerodynamics and Sonic Boom Mitigation," Paper AIAA-2001-3062, AIAA Plasmadynamics and Lasers Conference and 4th Weakly Ionized Gases Workshop, Anaheim, CA, June 11-14, 2001.
11. B. McAndrew, R. Murray, M. Shneider, R. Miles, J. Kline and J. Fox, "Comparison of Numerical and Experimental Results from Localized Microwave-Driven Plasma Energy Addition into a Mach 3 Flow," Paper AIAA-2001-3061, AIAA Plasmadynamics and Lasers Conference and 4th Weakly Ionized Gases Workshop, Anaheim, CA, June 11-14, 2001.
12. R.B. Miles, S.O. Macheret, and M.N. Shneider, "High Efficiency, Nonequilibrium Air Plasmas Sustained by High Energy Electrons," Paper #869, PPPS-2001, ICOPS 2001, Las Vegas, NV, June 17-22, 2001.
13. S.O. Macheret, M.N. Shneider, and R.B. Miles, "Dynamics of Plasmas Sustained by Repetitive Ultrahigh Voltage DC or Subpicosecond Laser Pulses," Paper #766, PPPS-2001, ICOPS 2001, Las Vegas, NV, June 17-22, 2001.
14. S. Zaidi, Z. Tang, and R.B. Miles, "Rubidium Filtered Thomson Scattering Measurement in an Atmospheric Pressure Argon Arc," Paper #339, PPPS-2001, ICOPS 2001, Las Vegas, NV, June 17-22, 2001.
15. X. Pan. L. Qian, M.N. Shneider, and R.B. Miles, "Plasma Measurements Using Ponderomotive Forces to Perturb the Translational Motion of Particles," Paper #340, PPPS-2001, ICOPS 2001, Las Vegas, NV, June 17-22, 2001.
16. M.N. Shneider, S.O. Macheret, and R.B. Miles, "Properties of Electron Beam Generated, Steady-State, Weakly Ionized Plasmas in Air," Paper #682, PPPS-2001, ICOPS 2001, Las Vegas, NV, June 17-22, 2001.

4.1.3 Dr. Walter Lempert

Senior Research Scientist
Mechanical and Aerospace Engineering Department

Phone:609-258-2875 |**FAX:**609-258-1139|**Email:**
walt@hepcat.princeton.edu

Degrees

B.S. (Chemistry), Lehigh University, 1975
Ph.D. (Physical Chemistry), University of Utah, 1981

Research Interests

Studies of fundamental spectroscopic phenomena and development of associated optical diagnostics. Laser development and nonlinear optics. Influence of collisional dynamics on spectral lineshapes. Optical propulsion. Recent activities include: Stimulated Raman scattering in oxygen and nitrogen; flow tagging velocimetry measurements in compressible and incompressible flow; spectrally filtered Rayleigh scattering velocimetry; development of pulse-burst Nd:YAG and robust injection-locking of Ti:Sapphire; use of high-power lasers for optical propulsion.

Selected Publications

1. J.H. Grinstead, N.D. Finkelstein, and W.R. Lempert, "Doppler Velocimetry in a Supersonic Jet Using Frequency-Modulated Filtered Light Scattering," *Opt. Lett.*, Submitted, October 1996.

2. R.B. Miles and W.R. Lempert, "Quantitative Flow Visualization in Unseeded Flows," *Annual Review of Fluid Mechanics*, (Invited), Submitted, May 1996.

3. A. Noullez, G. Wallace, W. Lempert, R.B. Miles, and U. Frisch, "Transverse Velocity Increments in Turbulent Flow Using the RELIEF Technique," *J. Fluid Mechanics*, Submitted, May 1996.

4. W.R. Lempert, K. Magee, P. Ronney, K.R. Gee, and R.P. Haugland, "Flow Tagging Velocimetry in Incompressible Flow Using Photo-Activated Nonintrusive Tracking of Molecular Motion (PHANTOMM)," *Expts in Fluids*, 18, pp. 249-257, 1995.

Principal Research Efforts

- The Radiatively-Driven hypersonic Wind Tunnel
- Flow tagging in air and water for fundamental studies of unsteady and turbulent flow
- Spectrally resolved scattering measurements using atomic and molecular vapor filters
- Development of high-power, pulse-burst laser sources for MHz rate imaging of high-speed phenomena
- Development of high power, single frequency laser sources for quantitative imaging diagnostics

4.1.4 Dr. Dennis K. Killinger

Professor, Physics, University of South Florida
Telephone: (813) 974-3995
E-mail: killinge@chuma.cas.usf.edu

Publications

P. Mamidipudi and D.K. Killinger, "Optimal Detector Selection for a 1.5-micron KTP OPO Atmospheric Lidar," SPIE Aerospace Pub. 3707, *Laser Radar Technology and Applications* (1999).

"Manufacturing Process Controls for the Industries of the Future," NRC Panel on Manufacturing Profcess Controls, Committee on Industrial Technology Assessments, *National Academic Press* (1998).

"Harnessing Light: Optical Science and Engineering in the 21st Century," *National Academy Press* (1998).

T. Taczak and D.K. Killinger, "Development of a tunable, narrow-linewidth CW 2.06-micron Ho:YLF laser for remote sensing of atmospheric CO2 and H2O," *Applied Optics*, 37, 8460 (1998).

G.W. Hagen, R.B. Streeter, D.K. Killinger, W.E. Swartz, "Florida's Tech Deployment Offsets Defense Downturn," *Forum for Applied Research and Policy, volume II*, p.75 (1996).

C. He and D.K. Killinger, "Dual-Polarization Modes and Self-Heterodyne Noise in a Single-Frequency 2.1 um Microchip Ho, Tm:YAG Laser," *Optics Letters*, 19, 396 (1994).

Y. Saito, K.P. Chan amd D.K. Killinger, "Development of an Eye-Safe LIDAR System Using 2.1 um Ho Laser," *The Review of Laser Engineering*, 22, 197 (1994).

M. Vaidyanathan and D.K. Killinger, "Absorption Strenght and Pressure Broadened Linewidth Measurements of the 1.73 um (2-0) Band of HCl at High Temperatures," *J. Quant. Spect. and Radiative Transfer*, 49, 659 (1993).

D.K. Killinger and R. Menzies, "Recent Advances in LIDAR/Laser Atmospheric Sensing," *IEEE LEOS Newsletter*, 7, 18 (1993).

M. Vaidyanathan and D.K. Killinger, "Tunable 1.7 um Laser Spectrometer for Optical Absorption Measurements of CH4, C2, H4 and High Temperature HCl," *Applied Optics*, 32, 847 (1993).

4.1.5 Dr. David A Krueger

Professor, Department of Physics, Colorado State University

B.S., Montana State University, 1961
Ph.D., University of Washington, 1967

krueger@lamar.colostate.edu (970) 491-7381

Research Interests

Lidar techniques have proven very versatile in the study of the space and time variation of atmospheric properties such as wind speeds and concentrations of ozone, pollutants, and aerosols. More recently interest has turned to developing techniques to measure air temperatures and densities. The basic difficulty is in separating the effects of aerosols from those of the air molecules. In our experiments shown schematically in the figure, a pulse (10 nsec) of nearly monochromatic light (~ 0.1 GHz) is sent into the atmosphere, and the spectrum of the scattered light is shown schematically as the heavy line. The light scattered by the aerosols is slightly Doppler-broadened due to the relatively low speeds of the aerosols (few m/sec) characteristic of the wind. The light scattered by the molecules has a much larger Doppler-broadening (~ 2.7 GHz) due to the relatively high speeds of the molecules (~ 500 m/sec). This Doppler-broadening is roughly proportional to the square root of the air temperature. The method utilizes three signals. The first two signals (shown in the figure) depend on the molecular scattering only and allows the determination of the air temperature and the air density if the atmosphere is assumed to be in hydrostatic equilibrium. This signal is obtained by using a band-stop vapor filter which will block essentially all of the light scattered by the aerosols. A typical transmission function is shown for an atomic vapor filter. Two slightly different vapor filters are used in channels 1 and 2. The third signal depends on both the molecular scattering and the aerosol scattering and is obtained by measurements without the filter. Subtracting the molecular scattering from the third signal allows determination of the aerosol scattering and thus properties such as aerosol density and shape distribution. In addition to providing a useful tool to atmospheric science in general, these air temperature and density profiles and the characterization of the aerosol properties are important in the analysis of other experiments on the processes of ozone depletion in the atmosphere.

4.1.6 Dr. Chiao-Yao (Joe) She

Professor, Colorado State University

B.S., Taiwan University, 1957
Ph.D., Stanford University, 1964
Fellow, Optical Society of America

(970) 491-6261, joeshe@lamar.colostate.edu

Research Interests

The research interests of Prof. She have been broad and often interdisciplinary. Over the past thirty years, he has been interested in the development of new laser techniques for specific applications on basic as well as applied problems. These included photon-burst fluorescence spectroscopy for single atom detection, coherent Raman spectroscopy for supersonic velocity and temperature measurements, Raman studies of surfaces and thin films. In 1980's, he initiated coherent Rayleigh-Brillouin gain spectroscopy, and pioneered the development of two types of narrowband lidars. Since the existing lidar technique for temperature measurements at the time relies on Rayleigh scattering for measuring air-density profiles from which the atmospheric temperatures are calculated, this approach fails for altitudes below 20 km and above 80 km due, respectively, to the interference of aerosol particles and to the lack of Rayleigh signal. His group remedies these short-comings by inventing new lidar techniques. For altitudes below 20 km, he uses a narrowband laser and a narrowband atomic vapor filter to separate molecular scattering from aerosol scattering so that air temperatures can be measured directly. For altitudes above 80 km, he uses a narrowband tunable laser to induce fluorescence emission of natural Na atoms existed in the mesopause region (between 80 to 110 km, a region too high for airplane and balloon and too low for satellite) for temperature measurements. Both systems are now capable of making atmospheric measurements. The narrowband Rayleigh-Mie lidar recently has provided the first simultaneously measured tropospheric temperature and aerosol extinction coefficient profiles at the popular doubled-YAG laser wavelength (532 nm). The Na temperature lidar based on a narrow-band dye laser system is being reproduced by other research groups. In addition, he has conceived and developed a single frequency coherent source at 589 nm based on sum-frequency generation, along with Na vapor Faraday filter, and acoustooptic frequency shifter permitting Na wind and daytime measurements.

Professor She's technical inventions have led to decade-long observation of the mesopause region in Fort Collins, Colorado which not only confirmed and detailed the predicted bizarre thermal structure with cold summer and warm winter, but also led to unexpected discoveries, linking climate change in this region to the Mt. Pinatubo eruption and solar flux variations, providing the first direct experimental evidence for the fact that different atmospheric layers and planetary space environment are strongly coupled as an integrated climatic system. To gain a basic understanding of this unique thermal structure, measurements of temperatures and winds, as well energy and momentum fluxes should be made from space as well as from the important polar region. For these reasons, Prof. She's lidar group has begun collaborative ground-based measurements in support of the TIMED (Thermosphere, Ionosphere, Mesosphere and Electrodynamics) satellite to be launched by NASA in 2001, and the deployment of a state-of-the-art Sodium lidar in ALOMAR (Arctic Lidar Observatory for Middle Atmospheric Research), Norway based on the Na fluorescence technology developed at Colorado State over the years with NSF support. In the latter case, the unique Faraday filter capable of rejecting sky light background is a must for observation in sunlit Arctic summer.

4.2 Sonar

4.2.1 Dr. Stanley E. Dunn

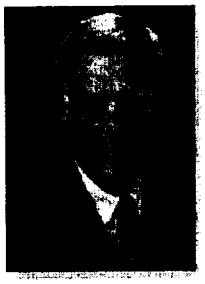

Professor
Department of Ocean Engineering
Florida Atlantic University
Boca Raton, FL 33431
Boca Raton Campus: (561)297-3437
SeaTech Campus: (954)924-7265
Fax: (561)297-3885
E-mail: dunn@oe.fau.edu

EDUCATION

- Ph.D. - M.E., North Carolina State University, 1970.
- B.S. - M.E., North Carolina State University, 1965.

RELATED EXPERIENCE

- 1988-1990: *Acting Dean*, College of Engineering, Florida Atlantic University.
- Chairman, NSF Joint US/UK Program in Ocean Engineering - Underwater Vehicles.
- NSF-NOAA Oceans 2000 Workshop - 1992.
- NSF Workshop on Science Applications for AUV's - 1991.
- NSF Workshop on AUV Technology Advancement - 1992.
- NOAA Committee in AI Technology for Sea Grant Program.
- Editor, 1992 Symposium on Autonomous Underwater Vehicle Technology.
- Reviewer for National Science Foundation (OEID), National Sea Grant Program,
- Transportation Research Board, ABET, UNH UUV Symposium.
- 1992 USJNR Organizer and Coordinator for South Florida (FAU).
- Board of Directors, 3rd International Submarine Races - June 1993.
- National Ocean Resource Technology Development Committee.
- Co-Chairman, US/UK Workshop on Ocean Technology - March 1994.
- NSF US/Taiwan Workshop on Ocean Resources - 1995.
- DOD Laboratory Infrastructure Capabilities Study, Ships, Submarines, and Watercraft,
- Phase I & II, Co-Chair - 1994-1995.
- Naval Surface Ship Technology Program, HM&E Integration Workshop- 1996.
- IOS Sensors and Platforms Review Group - 1996.
- National Research Council Naval Studies Board Panel, Technology for Future Naval Forces - 1996.
- NSF Russia-US Workshop on Oceans and Oceans/Atmosphere - 1996.
- Engineering Accreditation Commission - 1996-97.

Consulting:

- FHWA, U.S. Navy, USEPA and a variety of other governmental and private parties.

HONORS AND AWARDS

- College Nominations for University Teacher of the Year - 1986.
- Engineer of the Year Award/Palm Beach County FES - 1990.
- Fellow, Florida Engineering Society - 1990.

RECENT PUBLICATIONS

Principal Publications of Last Five Years: 22 publications, of which the following are most recent:

- "Ocean Engineering Systems for Ocean Resources in Deep Sea Water", US/Taiwan Workshop, Taipei, Taiwan, 1995.
- "The Ocean Explorer AUV: A Modular Platform for Coastal Sensor Development", with S. Smith, Autonomous Vehicles in Marine Countermeasure Symposium, Naval Postgraduate School, Monterey, CA, April 4-7, 1995.
- "Integrated Sensor of UUV Technologies for Coastal Ocean Application", with S. Smith, P. Betzer and T. Hopkins, COSU'95, Yokohama, Japan, May 1995.
- "Ocean Engineering at Florida Atlantic University: A Program Expanding to Meet New Challenges", with S. Smith, MTS Journal, Vol. 26, No. 1, pp. 7-13, Spring 1992.
- "Intelligent Systems Design in Ocean Engineering", with S. Smith and P. Ananthakrishnan, Proceedings of 1995 ASEE Annual Conference, Anaheim, CA, June 1995, pp. 2840-2846.
- "A Quantitative Measure of Sea-State Effect on Small Autonomous Underwater Vehicle Motion in Shallow Water", P.E. An, G. Leavitt, S. Smith, and S. Dunn, Oceanology Int. 96, pp. 211-233, Brighton, UK, March 1996.
- "Data Collection with Multiple AUVs for Coastal Oceanography", S. Smith, S. Dunn, and E. An, Oceanology Int. 96, pp. 263-279, Brighton, UK, March 1996.
- "Multi-Sensor Data Fusion for AUV Navigation in Shallow Water", P. E. An, A. Healey, S. Smith, and S. Dunn, IEEE AUV '96, Monterey, CA, June 1996.
- "Strategies for Simultaneous Multiple AUV Operation and Control", S. Smith, K. Ganesan, S. Dunn, and P. An, IARP 96, France, 1996.
- "Development of Autonomous Underwater Vehicles Based Survey and Sampling Capabilities for Coastal Exploration", with S. Smith, K. Ganesan, and E. An, Oceans '96 MTS/IEEE, 23-26 September 1996, Ft. Lauderdale, FL.
- **Book Chapter:** "Design of AUVs for Coastal Oceanography", with S. Smith, P. Betzer, T. Hopkins, Chapter 12, Underwater Robotic Vehicles, J. Yuh, Ed., TSI Press, pp. 299-326, 1995.

SCIENTIFIC AND PROFESSIONAL SOCIETIES

- American Society of Electrical Engineers (ASEE)
- Acoustical Society of America (ASA)
- Institute of Noise Control Engineering (INCE)
- Society of Naval Architects and Marine Engineers (SNAME)
- American Society of Mechanical Engineers (ASME)
- Institute of Electrical and Electronic Engineers (IEEE)

4.3 Raman

4.3.1 NASA JSC

4.3.2 NASA GRC (W. A. de Groot)

4.3.3 NASA Stennis

4.3.4 NASA MSFC (W. T. Powers)

4.3.5 Dr. Michael D. Hampton

Associate Professor, Department of Chemistry, University of Central Florida

Education:

Ph.D. Analytical Chemistry, Texas Tech University, 1980
B.S. Chemistry, University of Florida, 1975

Research Interests:

Hydrogen storage systems, ion selective electrodes, piezoelectric oscillators as chemical oscillators, materials (inorganic).

Selected Publications:

Michael D. Hampton and Janice K. Lomness, "Water Activation of Mg2Ni for Hydrogen Uptake", International Journal of Hydrogen Energy, (submitted Sept. 5,1997) accepted Jan., 1998, in press.

Michael P. McCann and Michael D. Hampton, Detection of Molecular Hydrogen by Stimulated Raman Emission, *Applied Spectroscopy*, 48(4), 537 (1994).

B. J. Lockhart, M. D. Hampton, C. J. Bryan, Symposium on Flammability and Sensitivity of Materials in Oxygen-Enriched Atmospheres: Fourth Volume, ASTM STP 1040, J. M. Stoltzfus, F. J. Benz, and J S. Stradling Ed., American Society for Testing and Materials, Philadelphia, PA, 1989.

M. D. Hampton, W. Rees, S. Hall, and J. L. Mills, "Trimethyl Borane." *Inorganic Syntheses*, 29, (1989).

M.D. Hampton, C.A. Peters, and L. Wellington, "Response of Poly(Vinyl Chloride) Electrodes Based on the Neutral Carrier 1,4,7,10-Tetraoxacyclododecane", *Analytica Chimica Acta*, 194, 171(1987).

Contact:

Phone: (407) 823-2136
E-mail: mhampton@ucflvm.cc.ucf.edu

4.3.6 *Myung K. Kim*

Associate Professor, Department of Physics, University of South Florida

Areas of Expertise

- digital holography; holographic microscopy
- nonlinear optics; coherent optical transient phenomena; photon echo; laser spectroscopy; quantum interference in atomic systems
- applications of photon echo in optical memory and optical processing; associative optical memory; pattern recognition

Education

- Ph.D. in Physics, Jun. 1986, University of California, Berkeley, CA
- B.S. in Physics and Mathematics, May 1979, Cum Laude, University of California, Los Angeles, CA

Employment History

- Associate Professor, Aug. 1995 - present, Dept. of Physics, University of South Florida, Tampa, FL
- Assistant Professor, Aug. 1988 - May, 1995, Dept. of Physics and Astronomy, Wayne State University, Detroit, MI
- Postdoctoral Fellow, Jan. 1986 - Aug. 1988, Chemical Physics Laboratory, SRI International, Menlo Park, CA

Refereed Journal Publications

- C.A. Cattel, M.K. Kim, R.P. Lin, and F.S. Moser, "Observations of large electric fields near the plasmasheet boundary by ISEE-1", Geophys. Res. Lett. **9**, 539 (1982).
- M.K. Kim and R. Kachru, "Long-term image storage and phase conjugation by a backward-stimulated echo in Pr3+:LaF3", J. Opt. Soc. Am. B **4**, 305 (1987).
- M.K. Kim and R. Kachru, "Storage and phase conjugation of multiple images using backward-stimulated echo in Pr3+:LaF3", Opt. Lett. **12**, 593 (1987).
- M. Mitsunaga, M.K. Kim, and R. Kachru, "Degenerate photon echoes: simultaneous storage of multiple optical data", Opt. Lett. **13**, 536 (1988).
- M.K. Kim and R. Kachru, "Multiple-bit long-term data storage by backward stimulated echo in Eu3+:YAl03", Opt. Lett. **14**, 423 (1989).
- M.K. Kim and R. Kachru, "Many-bit optical data storage by backward stimulated echo", Appl. Opt. **28**, 2186 (1989).
- M.K. Kim and R. Kachru, "Hyperfine measurements of 1D2 - 3H4 transition in Pr3+:YAG using photon echo", Phys. Rev. B **40**, 2082 (1989).
- M. Mitsunaga, R. Kachru, E. Xu, and M.K. Kim, "cw photon echo", Phys. Rev. Lett **63**, 754 (1989).
- E.Y. Xu, S. Kröll, D.L. Heustis, R. Kachru, and M.K. Kim, "Nanosecond image processing using stimulated photon echoes", Opt. Lett. **15**, 562 (1990).
- S. Kröll, E.Y. Xu, M.K. Kim, M. Mitsunaga and R. Kachru, "Intensity-dependent photon echo relaxation in Pr3+:YAG", Phys. Rev. B **41**, 11568 (1990).

- M.K. Kim and R. Kachru, "Hyperfine structures of praseodymium ions in solids using stimulated photon echo modulation", Phys. Rev. B **44**, 9826 (1991).
- D. Manganaris, P. Talagala and M. K. Kim, "Spatial mixed binary multiplication by photon echoes", Appl. Opt. **31**, 2426 (1992).
- R.A. Breitenbach, P.K. Swisher, M.K. Kim, and B. S. Patel, "The photic sneeze reflex as a risk factor to combat pilots", Military Medicine **158**, 806 (1993).
- Y. Zhao, C. Wu, P. Shah, M.K. Kim, and L.R. Dawson, "Experimental observation of optical phase conjugation in InGaAs/GaAs multiple quantum wells at 1.06 μm wavelength", Appl. Phys. Lett. **63**, 281 (1993).
- P.R. Hemmer, S.M. Shahriar, M.K. Kim, K.Z. Cheng, and J. Kierstead, "Time domain optical data storage using Raman coherent population trapping", Opt. Lett. **19**, 296 (1994).
- B.S. Ham and M.K. Kim, "Photon-echo amplification by an external-cavity amplifier", Appl. Opt. **33**, 4472 (1994).
- P. Talagala, S.H. Ling, and M.K. Kim, "Photon echoes using broadband cw laser", J. Mod. Opt. **43**, 253 (1996).
- P.R. Hemmer, M.S. Shahriar, B.S. Ham, M.K. Kim, and Yu. Rozhdestvensky, "Optical spectral holeburning with Raman coherent population trapping", Molecular Crystals and Liquid Crystals **291**, 287 (1996).
- Y. Zhao, C. Wu, B.S. Ham, M.K. Kim, and E. Awad, "Microwave induced transparency in ruby", Phys. Rev. Lett. **79**, 641 (1997).
- B.S. Ham, M.S. Shahriar, M.K. Kim, and P.R. Hemmer, "Frequency-selective time-domain optical data storage by electromagnetically induced transparency in a rare-earth doped solid", Opt. Lett. **22**, 1849 (1997).
- H. Sonajalg and M.K. Kim, "Perturbation analysis of Raman echo", J. Opt. Soc. Am. B **15**, 1780 (1998).
- B. S. Ham, M. S. Shahriar, M. K. Kim, and P. R. Hemmer, "Spin coherence excitation and rephasing with optically shelved atoms", Phys. Rev. B **58**, R11825-R11828 (1998).
- B.S. Ham, P.R. Hemmer, M.K. Kim, and S.M. Shahriar, "Quantum interference and its potential applications in a spectral hole-burnign solid", Laser Physics **9**, (3) (1999).
- M.K. Kim, "Wavelength scanning digital interference holography for optical section imaging", Opt. Lett. **24**, 1693 (1999)
- M.K. Kim, B.S. Ham, P.R. Hemmer, and M.S. Shahriar, "Observation of sub-kilohertz resonance in rf-optical double resonance experiment in rare earth inos in solids", J. Mod. Opt. 47, 1713-1728 (2000)

4.4 Schlieren

4.4.1 Dr. Robert E. Peale

Associate Professor of Physics
School of Optics/CREOL
Electrical and Computer Engineering
Advanced Materials Processing and Analysis Center (AMPAC)

404 MAP, (407) 823-5208
rep@physics.ucf.edu
http://www.physics.ucf.edu/~rep

B.S. 1983 (UC Berkeley),
M.S. 1986, Ph.D. 1990 (Cornell)

Dr. Peale's research accomplishments span a wide range of topics. These include defects in semiconductors, spectroscopic and optical instrumentation, rare-earth activated optical materials, and far-infrared semiconductor lasers. Recent interests include semiconductor-device process integration and basic science related to nuclear waste remediation.

Research

Current projects include mode-locking of the p-Ge far-infrared laser, solution growth of calcite single crystals, sputter growth of InAs thin films, and deep ion implantation for device processing.

Selected Publications

"Zebra schlieren optics for leak detection," R. E. Peale and P. L. Summers, Appl. Opt. 35, 4518 (1996).

"Evidence for self-mode-locking in p-Ge laser emission," A. V. Muravjov, R. C. Strijbos, C. J. Fredricksen, H. Weidner, W. Trimble, S. H. Withers, S. G. Pavlov, V. N. Shastin, and R. E. Peale, Appl. Phys. Lett. 73, 3037 (1998).

"Pulse separation control for mode-locked far-infrared p-Ge lasers," A. V. Muravjov, R. C. Strijbos, C. J. Fredricksen, S. H. Withers, W. Trimble, S. G. Pavlov, V. N. Shastin, and R. E. Peale, Appl. Phys. Lett. 74, 167 (1999).

"Broad band p-Ge optical amplifier of terahertz radiation," A. V. Muravjov, S. H. Withers, S. G. Pavlov, V. N. Shastin, and R. E. Peale, J. Appl. Phys 86, 3512 (1999).

"Actively mode-locked p-Ge laser in Faraday configuration," A. V. Muravjov, S. H. Withers, R. C. Strijbos, S. G. Pavlov, V. N. Shastin, and R. E. Peale, Appl. Phys. Lett. 75, n19 (1999).

4.4.2 Dr. DeVon W. Griffin

NASA GRC
Devon.W.Griffin@grc.nasa.gov

4.5 Fourier Transform Infrared

4.5.1 Thomas J. Kulp

Sandia National Laborarories, Combustion Research Facility
Phone: (925) 294-3676
Email: tjkulp@sandia.gov
Fax: (925) 294-2595
Mail Stop: 9056

5 EXTEND DIFFUSION MODEL

5.1 Basic Model

In order to evaluate the various technologies for leak location, it is desirable to have a model (or map) of concentration of H_2 or He as a function of leak rate, distance from the leak, and time since the leak initiated. For the case of a leak into an open area, diffusion follows Fick's first law, expressed in one dimension as:

$$J_x = -D\left(\frac{\partial C}{\partial x}\right)$$

where, J_x refers to the molar flux in the x-direction in mol $m^{-2} s^{-1}$, C is the molar concentration in mol m^{-3} and, D is the diffusion coefficient or diffusivity in $m^2 s^{-1}$. In three dimensions in polar coordinates, this leads to the differential equation:

$$\frac{\partial C(r,t)}{\partial t} = D\frac{1}{r^2}\frac{\partial}{\partial r}(r^2\frac{\partial C(r,t)}{\partial r})$$

where r is the radius from the leak, and t is the time since initiation of the leak. With appropriate boundary conditions:

$$C(r,t) = 0 \quad \text{for } t<0$$
$$C(r,0) = \delta(r)$$
$$C(\infty,t) = 0$$

where δ is the *Kronecker delta* function, the solution[4] is:

$$C(r,t) = \frac{\phi}{4\pi Dr} efrc\,[\frac{r}{\sqrt{4Dt}}]$$

where ϕ is the leak rate in mol/s, and *erfc* is the complimentary error function[5]:

$$erfc(x) = \frac{2}{\sqrt{\pi}}\int_x^\infty e^{-\xi^2} d\xi$$

An interactive version of this model has been provided in the form of a *MathCAD* worksheet.

For the steady state case $t \rightarrow \infty$ and the concentration reduces to:

$$C(r) = \frac{\phi}{4\pi Dr}$$

The diffusion coefficients for gas 1 in gas 2 is given by the Fuller equation[6]:

$$D_{1,2} = \frac{0.604 \times 10^{-8} \bullet T^{1.81} \bullet \left[\frac{M_1 + M_2}{M_1 M_2}\right]^{0.5}}{p\left(T_{c,1} T_{C,1}\right)^{0.1405}\left(V_{c,1}^{0.4} + V_{c,2}^{0.4}\right)^2}$$

where:

M_1, M_2 : molecular weight of both components in kg/kmol;

$T_{c,1}$, $T_{c,2}$: critical temperature in K;

$V_{c,1}$, $V_{c,2}$: critical volume in m^3/kmol ($V_c = M/(1000 d_c)$)

T: temperature in K;

P: pressure in bar (1bar = 0.98692 atm) ;

$D_{1,2}$: diffusion coefficient of gas 1 in gas 2 in m^2/s

The critical properties for selected gases[7] are given in Table 8:

Table 8: Critical data for selected gases

Gas	T_c [K]	P_c [bar]	d_c [g cm^{-3}]	MW [kg $kmol^{-1}$]
air	132	3.77	0.316	29
H_2	33.2	1.29	0.031	2.02
He	5.19	0.23	0.070	4.003
N_2	126.2	3.39	0.313	28.01
O_2	154.7	5.04	0.436	32.00

Therefore, at a temperature of 25°C and pressure of 1 atm:

$$D_{H2\text{-}Air} = 7.78 \text{ x } 10^{-5} \text{ m}^2/\text{s}$$

$$D_{He\text{-}Air} = 7.73 \text{ x } 10^{-5} \text{ m}^2/\text{s}$$

A basic diffusion model was developed in Phase 1. Sample results from this model are given in Figure 11, which shows the molar fraction in percent (equivalent to percent concentration by volume) as a function of distance from the leak for an H_2 leak at 10^{-2} SCIM after 1 s, 1 min, 1 h, and for steady state. The concentration is linearly proportional to the leak rate, so the *form* of the curves is the same for all leak rates; changing the leak rate effectively changes only the scale of the y axis. The diffusion coefficient for He is very close to that for H_2, so the graph for He is virtually the same.

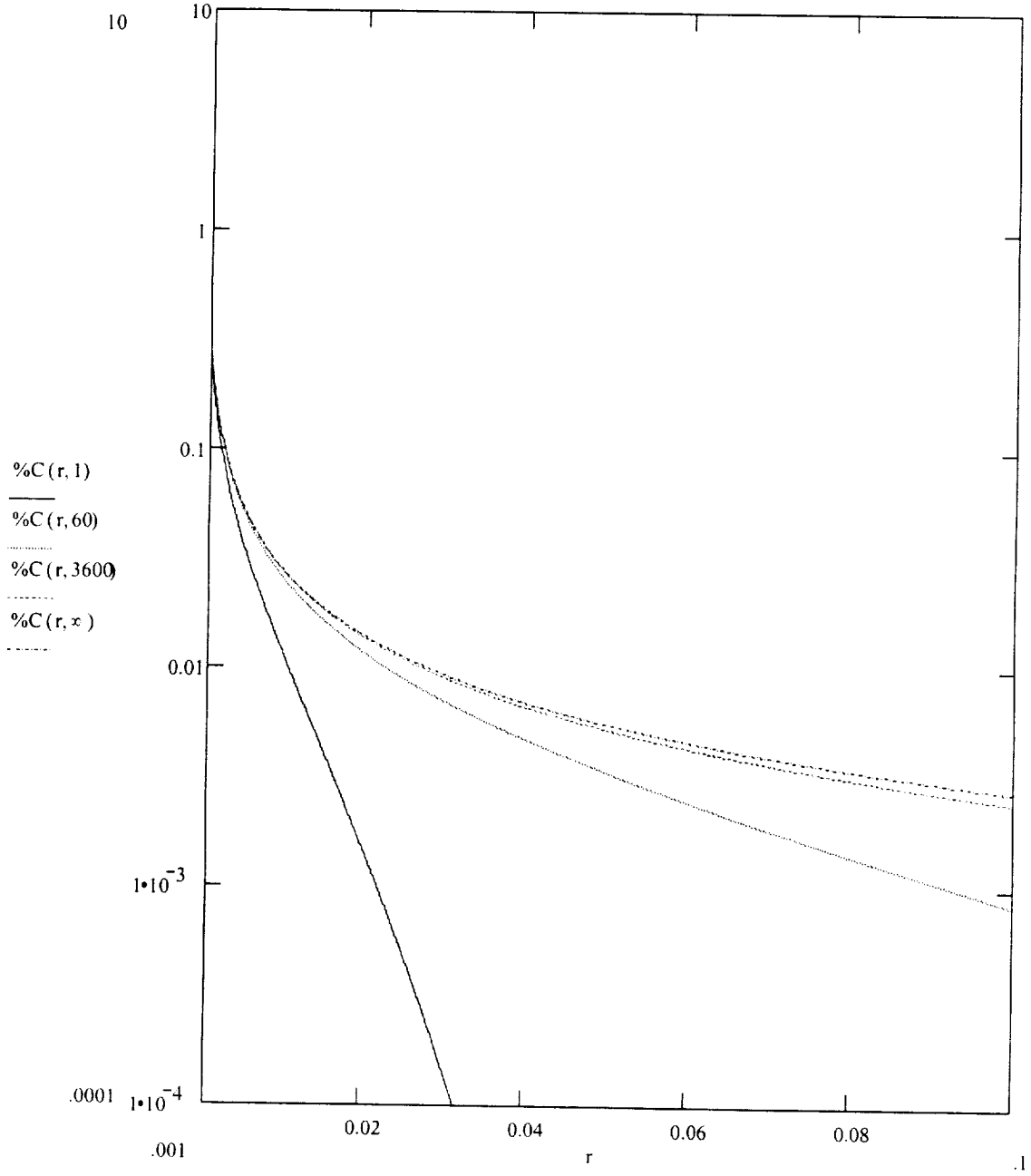

Figure 11: Concentration of H_2 [mol fraction] vs. distance [m] for a leak of 10^{-2} SCIM, at 1 s, 1 min, 1 h, and steady state

5.2 Extended Model

In Phase 2, we extended the model to include the effects of gravitational convection and forced convection. Gravitational convection refers to the tendency for lighter gases to rise and heavier gases to sink. Forced convection refers to air currents from wind or ventilation. The steady-state velocity for gravitational convection is given by the Ernst Einstein equation:

$$v_z = \frac{F_z * D}{\kappa * T}$$

where the net force F_z is given by

$$F_Z = (m_{air} * g) - (m_{gas} * g)$$

In these equations, F_z is the net force acting on the body in the Z direction, κ is the Boltzmann constant (1.38 x 10^{-22} N m / °K), T is temperature in Kelvin, g is the acceleration due to gravity in m/s^2.

Forced convection can result in flow that is laminar or turbulent. The characteristics of turbulent flow are highly dependant on the details of the source of the convection and the dimensions and characteristics of the surroundings, so this model simulates only laminar flow.

Convection breaks the spherical symmetry used to simplify the problem in the basic model. The extended model uses Cartesian coordinates and solves the resulting differential equations numerically rather than analytically. A finite difference approach is used to solve the partial differential equations. This approach divides the volume into a grid in x, y, z and time.

The generalized three-dimensional equation for diffusion is given by Fick's second law:

$$\frac{\partial c}{\partial t} = D\frac{\partial^2 c}{\partial x^2} + D\frac{\partial^2 c}{\partial y^2} + D\frac{\partial^2 c}{\partial z^2}$$

The volume is divided into a grid and the step in each direction is given by:

$$x = i\delta x,\ y = j\delta y,\ z = k\delta z, t = l\delta t$$

where i, j, k, l are positive integers in x, y, z & t directions.

Using Taylor's series expansion for the partial differential, one obtains:

$$C_{i,j,k+1} = C_{i,j,k} + D\frac{\delta t}{(\delta x)^2}\left[C_{i+1,j,k,l} - 2C_{i,j,k,l} + C_{i-1,j,k,l}\right]$$
$$+ D\frac{\delta t}{(\delta y)^2}\left[C_{i,j+1,k,l} - 2C_{i,j,k,l} + C_{i,j-1,k,l}\right]$$
$$+ D\frac{\delta t}{(\delta z)^2}\left[C_{i,j,k+1,l} - 2C_{i,j,k,l} + C_{i-1,j,k-1,l}\right]$$

The criterion for a stable solution is:

$$D\left[\frac{1}{\delta x^2} + \frac{1}{\delta y^2} + \frac{1}{\delta z^2}\right]\delta t \le 1/2$$

When forced convection along the x-axis and gravitational convection along the z-axis are added, the differential equation becomes:

$$\frac{\partial c}{\partial t} = D * \nabla^2 c - \nabla(c.v_z) - \nabla(c.v_c)$$

The generalized finite difference kernel is then:

$$C_{i,j,k+1} = C_{i,j,k} + D\frac{\delta t}{(\delta x)^2}\left[C_{i+1,j,k,l} - 2C_{i,j,k,l} + C_{i-1,j,k,l}\right]$$
$$+ D\frac{\delta t}{(\delta y)^2}\left[C_{i,j+1,k,l} - 2C_{i,j,k,l} + C_{i,j-1,k,l}\right]$$
$$+ D\frac{\delta t}{(\delta z)^2}\left[C_{ij,k+1,l} - 2C_{ij,k,l} + C_{i-1j,k-1,l}\right]$$
$$- v_{gz}\frac{\delta t}{\delta z}\left[C_{i,j,k+1,l} - C_{i,j,k,l}\right]$$
$$- v_x\frac{\delta t}{\delta x}\left[C_{i+1,j,k,l} - C_{i,j,k,l}\right]$$
$$- v_y\frac{\delta t}{\delta y}\left[C_{i,j+1,k,l} - C_{i,j-1,k,l}\right]$$
$$- v_z\frac{\delta t}{\delta z}\left[C_{i,j,k+1,l} - C_{i,j,k,l}\right]$$

where v_{gz} is the gravitational convection velocity and v_x, v_y, v_z are the components of the forced convection velocity.

6 REFERENCE CITATIONS

[1] Robert Youngquist, private communication.

[2] R. M. Measures, *Laser Remote Sensing Fundamentals and Applications*, pp.98-99, Wiley – Interscience, New York (1984).

[3] D.R. Lide, *ed.*, *Handbook of Chemistry and Physics, 71st ed.*, p. 14-19, CRC Press (1991)

[4] H.S.Carslaw and J.C. Jaeger, *Conduction of Heat in Solids, 2nd ed.*, p. 261, Oxford (1959).

[5] J. Crank, *The Mathematics Of Diffusion*, p. 19 & Table 2.1, Oxford (1964).

[6] http://chemengineer.about.com/science/chemengineer/library/weekly/aa072197.htm

[7] H.W. Liepmann and A. Roshko, *Elements of Gasdynamics*, John Wiley & Sons (1957).

7 APPENDICES

7.1 NASA Technology Readiness Levels

Level 1	Basic principles observed and reported
Level 2	Technology concept and/or application formulated
Level 3	Analytical & experimental critical function and/or characteristic proof-of-concept
Level 4	Component and/or breadboard validation in laboratory environment
Level 5	Component and/or breadboard validation in relevant environment
Level 6	System/subsystem model or prototype demonstration in relevant environment
Level 7	System prototype demonstration in relevant environment
Level 8	Actual system completed and "Flight Qualified" through test and demonstration
Level 9	Actual system "Flight Proven" through successful mission operations

7.2 Bibliography

7.2.1 References Included in the Appendix

1. R. G. Seasholtz and L. C. Greer III, "Rayleigh Scattering Diagnostic for Measurement of Temperature and Velocity in Harsh Environments," *NASA/TM – 1998-206980* (1998).
2. R. G. Seasholtz and A. E. Buggele, "Improvement in Suppression of Pulsed Nd:YAG Laser Light With Iodine Absorption Cells for Filtered Rayleigh Scattering Measurements," *NASA Technical Memorandum 11317* (1997).
3. R. G. Seasholtz, A. E. Buggele, and M. F. Reeder, "Technical Support package – Measuring Flow Using Spectrally Resolved Rayleigh Scattering," *NASA Tech Briefs LEW-16425.*
4. P. Gölz and P. Andresen, "Atomic vapor filer for two-dimensional Rayleigh imaging experiments with a narrow-band KrF excimer laser," *Applied Optics* **35**(30), 6054-6061 (1996).
5. G. Tenti, C. D. Boley, and R. C. Desai, " On the Kinetic Model Description of Rayleigh – Brillouin Scattering from Molecular Gases," *Canadian Journal of Physics* **52**(4), 285-290 (1974).
6. R. B. Miles, W. R. Lempert, and J. N. Forkey, "Laser Rayleigh Scattering," *Measurement Science and Technology* **12**, R33-R51 (2001).
7. J.N. Forkey, N.D. Finkelstein, W. R. Lempert, and R. B. Miles, " Demonstration and Characterization of Filtered Rayleigh Scattering for Plannar Velocity Measurements," *AIAA Journal* **34**(3), 442-448 (1996).
8. R. G. Seasholtz and A. E. Buggele, "Study of Injection of Helium Into Supersonic Air Flow Using Rayleigh Scattering," *NASA Technical Memorandum 107409 AIAA-97-0155* (1997).
9. R. G. Seasholtz, A. E. Buggele, and M. F. Reeder, " Flow Measurements Based on Rayleigh Scattering and Fabry – Perot Interferometer," *Optics and Laser in Engineering* **27**, 543-570 (1997).
10. R. G. Seasholtz, A. E. Buggele, and M. F. Reeder, "Instantaneous Flow Measurements in a Supersonic Wind Tunnel Using Spectrally Resolved Rayleigh Scattering," *NASA Technical Memorandum 107042* (1995).
11. R. G. Seasholtz, F. J. Zupanc, and S. J. Schneider, " Spectrally Resolved Rayleigh Scattering Diagnostic for Hydrogen – Oxygen Rocket Plume Studies," *Journal of Propulsion and Power*, **8**(5), 935-942 (1992).
12. Shardanand and A. D. Prasas Rao, " Absolute Rayleigh Scattering Cross Sections of Gases and Freons of Stratospheric Interest in the Visible and Ultraviolet Regions," *NASA Technical Note NASA TN D-8442* (1977).
13. H. E. Kourous and R. G. Seasholtz, "Fabry – Perot Interferometer Measurement of Static Temperature and Velocity for ASTOVL Model Tests," *NASA Technical Memorandum 107014* (1994).
14. Z. Liu, I. Matsui, and N. Sugimoto, "High-spectral-resolution lida using an iodine absorption filter for atmospheric measurements," Optical Engineering, 38(10), 1661-1670 (1999).
15. L. D. Reynolds and C. B. Shaw, "Experimental method for gas kinetic tempture measurements in a thermal plasma," SPIE, 1554B, 622-631 (1991).
16. K. P. Chan and D. K. Killinger, "Short pulse coherent Doppler Nd:YAG lidar," Optical Engineering, 30(1), 49-54 (1991).
17. W. A. de Groot and F. J. Zupanc, "Laser Rayleigh and raman diagnostics for small hydrogen/oxygen rockets," SPIE, 1862, 98-112 (1993).

7.2.2 Additional References

- R. G. Sellar and D. Wang, *Assessment of Remote Sensing Technologies for Location of Hydrogen and Helium leaks, Phase 1 Final Report*, NAG10-0290 (2000).
- R. M. Measures, *Laser Remote Sensing Fundamentals and Applications*, Wiley – Interscience, New York (1984).
- J.N. Forkey, *Development and Demonstration of Filtered Rayleigh Scattering – A Laser Based Flow Diagnostic for Planar Measurement of Velocity, Temperature, and Pressure,* Final Technical Report for NASA Graduate Student Researcher Fellowship Grant NGT-50826 (1996).
- J. Crank, *The Mathematics of Diffusion*, Oxford Science Publication, second edition (1989)
- D.R. Poirier and G.H. Geiger, *Transport Phenomenon in Materials Processing*, TMS Publication (1994)
- R.E Cunningham and R.J.J. Williams, *Diffusion in Gases and Porous Media*, Plenum Press (1980)
- J. C. Strikwerda, *"Finite Difference Schemes and Partial Differential Equations"*, Wadsworth & Brooks/Cole.
- R. Taylor and R. Krishna, *" Multi-component Mass Transfer"*, John Wiley Series (1993)
- R.L. Burden and J. D. Faires, *"Numerical Analysis: Fourth Edition", PWS Kent* (1988)
- R.W. Fox and A.T. McDonald, *"Introduction to Fluid Mechanics: Third Edition"*, Wiley (1985)
- R.B. Bird, W.E. Stewart and E. N. Lightfoot, *"Transport Phenomena"*, Wiley, (1960)
- M. Zhu, H. Miyata and H. Kajitani, " Finite difference simulation of a viscous flow about a ship of arbitrary configuration", *The Proceedings: Fifth International Conference on Numerical Ship Hydrodynamics,* pp. 119-132 (1990)